3

Characterization of the Temporal Stability of ToM and Pain Functional Brain Networks Carry Distinct Developmental Signatures during Naturalistic Viewing

3.1 INTRODUCTION

Theory-of-Mind (ToM) is an evolving ability that significantly impacts human learning and cognition and is highlighted in 1978 by Premack and Woodruff Westby and Robinson [2014]; Premack and Woodruff [1978]. The ToM ability allows individuals to comprehend other people's aims, ambitions, and thinking that differ from their own Bhavna *et al.* [2023a].The ToM network primarily involves the medial prefrontal cortex (mPFC), temporoparietal junction (TPJ), posterior superior temporal sulcus (pSTS), and precuneus. Recent studies have primarily focused on understanding the development of ToM functions from the preschool age group and its association with middle childhood and early adolescence and characterized individual differences Devine and Apperly [2022]. According to the literature, children develop the ability to understand aim and intention and predict another person's actions in false belief task paradigms by the age of 4 years Devine and Apperly [2022]; Richardson *et al.* [2018]; Astington and Edward [2010]; Bartsch and Wellman [1995]. Hence, children's performance in explicit false belief tasks could index an important milestone in understanding concepts during ToM development, as theories of others' internal states are dramatically altered by insight into the representational nature of mental states. Analyzing the early age group data allows us to examine the development of the ToM network and re-examine the literature about children's ToM functional brain networks during naturalistic movie-watching tasks. Using naturalistic stimuli enables us to identify age-specific patterns in brain connectivity and how these patterns change as children grow, helping us track developmental trajectories in neural connectivity and their implications for cognitive processing. The human brain is a collection of massive functional modules that become more distinct during development from childhood to adolescence, i.e., connectivity within modules increases as we grow from childhood to adolescence, and connectivity between modules decreases Fair *et al.* [2009]; Gu *et al.* [2015]; Dosenbach *et al.* [2010]; Satterthwaite *et al.* [2013]. Therefore, previous studies have focused on functional connectivity measures within and between ToM and pain brain networks to address children's early developmental differences and functional specialization from 3-12 yrs and, subsequently, employed within and between-network functional connectivity measures to relate to performance in explicit false belief reasoning tasks Richardson *et al.* [2018]. Moreover, previous studies have reported a striking division between regions responding preferentially to internal states of others' bodies (like hunger, pain, and mental states) versus internal states (like beliefs and desires) of others' minds, suggesting a division of labor and early segregation into functionally specialized brain regions Kana *et al.* [2015]; Richardson *et al.* [2018]. Recently, dynamic functional connectivity (DFC) and temporal stability of DFC have emerged as a major topic in the resting-state BOLD functional magnetic resonance imaging (fMRI) literature Li *et al.* [2020a]; Zhang *et al.* [2016]; Sastry *et al.* [2022]. DFC captures fluctuation in temporal scale of minutes that contain meaningful information Sastry *et al.* [2022]; Harlalka *et al.* [2019]. While the participants are experiencing naturalistic stimuli, fluctuations and stochasticity inherent in temporal dynamics of DFC may

be crucial in shaping slow neuronal dynamics of ToM brain regions; on the contrary, a stable representation of temporal dynamics and corresponding stability of FC patterns over time are crucial for functional development of the cortex Li *et al.* [2020a]. In this context, which are the key contributors that sculpt the stability of dynamic FC patterns during tasks, and how they associate with different salient stimuli present in the movie clips (e.g., hunger, pain, and internal states like belief and desires) are vital questions to address. To this end, systematic quantitative characterization of the temporal stability measure that captures the variability or consistency of neural activity patterns over time (i.e., less temporal stability means more variability and vice-versa) and coordination between functionally specialized brain regions across neurodevelopment remain unexplored. Previous studies investigated the differences in temporal stability of functional architecture in the resting states of patients with neurological disorders and healthy controls and examined the effects of various activities Li *et al.* [2020a]; Zhang *et al.* [2016]; Sastry *et al.* [2022]. The studies also demonstrated that variable alterations in the functional architecture of the default mode network (DMN), visual and subcortical brain areas, which were specific to some neurological disorders (e.g., ADHD, schizophrenia, and autism spectrum disorder)Li *et al.* [2020a]; Zhang *et al.* [2016]; Sastry *et al.* [2022]. Therefore, existing neuroimaging studies leave a gap in addressing fundamental questions of interest concerning temporal stability in the early stages of development in the ToM functional brain networks and their association with behavior.

Recent evidence suggests that during ToM-related tasks, neural activation is found predominantly in the Bilateral Temporoparietal Junction (Left TPJ and Right TPJ), Medial Prefrontal Cortex, and Posterior Cingulate Cortex using fMRI data; however, it remains unknown at which stage of neurodevelopment the temporal stability of these regions undergoes alterations Kana *et al.* [2015]. Moreover, there are no existing studies that quantify whether the temporal stability of social brain regions of ToM and Pain (sensory) networks carry distinct or overlapping signatures during naturalistic stimulus processing in children during development and whether the pattern of temporal stability indicates the successful development of ToM reasoning ability thus far. Secondly, whether the temporal stability patterns of social brain regions of ToM in 3-12 yrs could associated with the performance in false belief reasoning tasks remains least understood Richardson *et al.* [2018]; Astington and Edward [2010]. According to our hypothesis, the aim of the present study is twofold: (1) to precisely characterize the temporal stability of ToM and Pain brain networks and age-associated differences in the stability and fluctuations from the early childhood stage to adolescence using a recently proposed novel unsupervised approach; (2) to identify whether temporal stability of ToM functional brain networks could be associated with success or failure in explicit false belief task performance in children and adults. Our findings contribute significantly to the ongoing understanding of the neural dynamics at the early developmental stage by focusing on ToM functional brain networks and the potential utility of their temporal stability as an associated measure with individual differences in false belief task performance

The thesis chapter is organized as follows: firstly, to test our hypothesis, we used an early childhood dataset comprising 122 participants (3-12 yrs age range) with 33 adult controls (total number of participants = 155) passively viewing a short, animated movie that included events evoking the mental states and physical bodily sensations of the clip characters while undergoing fMRI. A recent study has validated this movie, which activates ToM brain regions and the pain regions Richardson *et al.* [2018]. To check how temporal stability differs between ToM and pain scenes and evolves in both cases upon aging, we used a data-driven unsupervised approach to capture high-dimensional dynamic functional connectivity (DFC) via low-dimensional patterns and subsequent estimation of temporal stability using quantitative metrics. The reason for using temporal stability instead of the traditional approaches was its ability to capture dynamic changes over time (even in a tiny instance), individual variability, and developmental trajectories. We use Angular and Mahalanobis distances to identify the ToM and Pain network temporal stability when movie stimuli/clips contain internal activation of mental and physical states activating brain

networks at specific moments in time. We have conducted the following analysis to address core questions regarding the temporal stability of functional brain networks (ToM and Pain) involved in representing internal mental and physical states. The brain regions associated with ToM and pain networks have been selected based on a previous study that reported 12 brain regions (refer to Table 7.1) Dufour *et al.* [2013]; Bruneau *et al.* [2015]; Richardson *et al.* [2018]. ToM brain regions include bilateral temporoparietal junction, precuneus, and middle, dorso- and ventromedial prefrontal cortices. The pain network comprises brain regions recruited when perceiving the physical pain and bodily sensations of others: bilateral medial frontal gyrus, insular cortex, secondary sensory cortex, and dorsal anterior middle cingulate cortex. As in previous studies, we collapse these brain regions across specific functions and use ToM and pain networks as regions generally recruited for reasoning about others' internal mental and physical states. The contribution of the current study is as follows: A) We used the dynamic functional connectivity (DFC) to quantify temporal stability using our previous approach Sastry *et al.* [2022] of functional brain networks in 3-12 yrs-old children. Subsequently, we estimated dominant DFC subspaces of ToM and Pain networks to quantify their separation at an early age. B) To further capture ToM network temporal stability, we quantified differences between the dominant DFC subspaces using two distinct measures: (i) Angular Distance and (ii) Mahalanobis Distance. Our results suggest that ToM and Pain networks achieve considerable temporal stability by the age of 5 years. C) Finally, we have tested whether the temporal stability of functional networks is associated with the performance of participants in false belief reasoning tasks based pass, fail, or give inconsistent groups, which is carried out by the 3-12 yrs-old participants outside the scanner. The analysis is performed for complete movie duration and additionally, we highlighted the temporal stability where movie clips evoked higher activation. Our finding grounded on derived temporal stability differences in functional brain networks during developmental age may aid in developing avenues to address questions related to distinct neural responses to others' minds and bodies that are present at a very early age and continue to develop after when children pass explicit false-belief tasks and throw fundamental insights into the development of ToM brain networks (refer to Figure 7.1).

3.2 PROPOSED APPROACH

3.2.1 fMRI Movie Watching Dataset and MRI Preprocessing

In the current study, we analyzed a dataset of 155 early childhood to adult participants available on the OpenfMRI database under the accession number ds000228 and was originally collected by the Richardson et al. group Richardson *et al.* [2018]. The childhood group consisted of 122 participants aged 3-12-yrs (mean age = 6.7 yrs, SD = 2.3, 64 females), complemented by 33 adults (mean age = 24.8 yrs, SD = 5.3, 20 females) Richardson *et al.* [2018]. All the participants were from the local community and had submitted written consent from parent/guardian. The data were collected with approval from the Committee on the Use of Humans as Experimental Subjects (COUHES) at the Massachusetts Institute of Technology. Participants watched a sound-less short animated movie called "Partly Cloudy" for a total duration of 5.6 minutes, and the stimuli were validated to activate ToM and pain regions Richardson *et al.* [2018]; Reher and Sohn [2009]; Astington and Edward [2010] (refer to Figure 7.2). A 3-Tesla Siemens Tim Trio scanner at the Athinoula A. Martinos Imaging Center at MIT was used to collect whole-brain structural and functional MRI data Keil *et al.* [2011]. Children under age 5-yrs used one of two custom 32-channel phased-array head coils made for younger (n = 3, M(s.d.) = 3.91(.42) yrs) or older (n = 28, M (s.d.) = 4.07(.42) yrs) children; all other participants used the standard Siemens 32-channel head coil. Richardson *et al.* [2018]. With a factor of three for GRAPPA parallel imaging, 176 interleaved sagittal slices of 1 mm isotropic voxels were used to get T1-weighted structural images (FOV: 192 mm for child

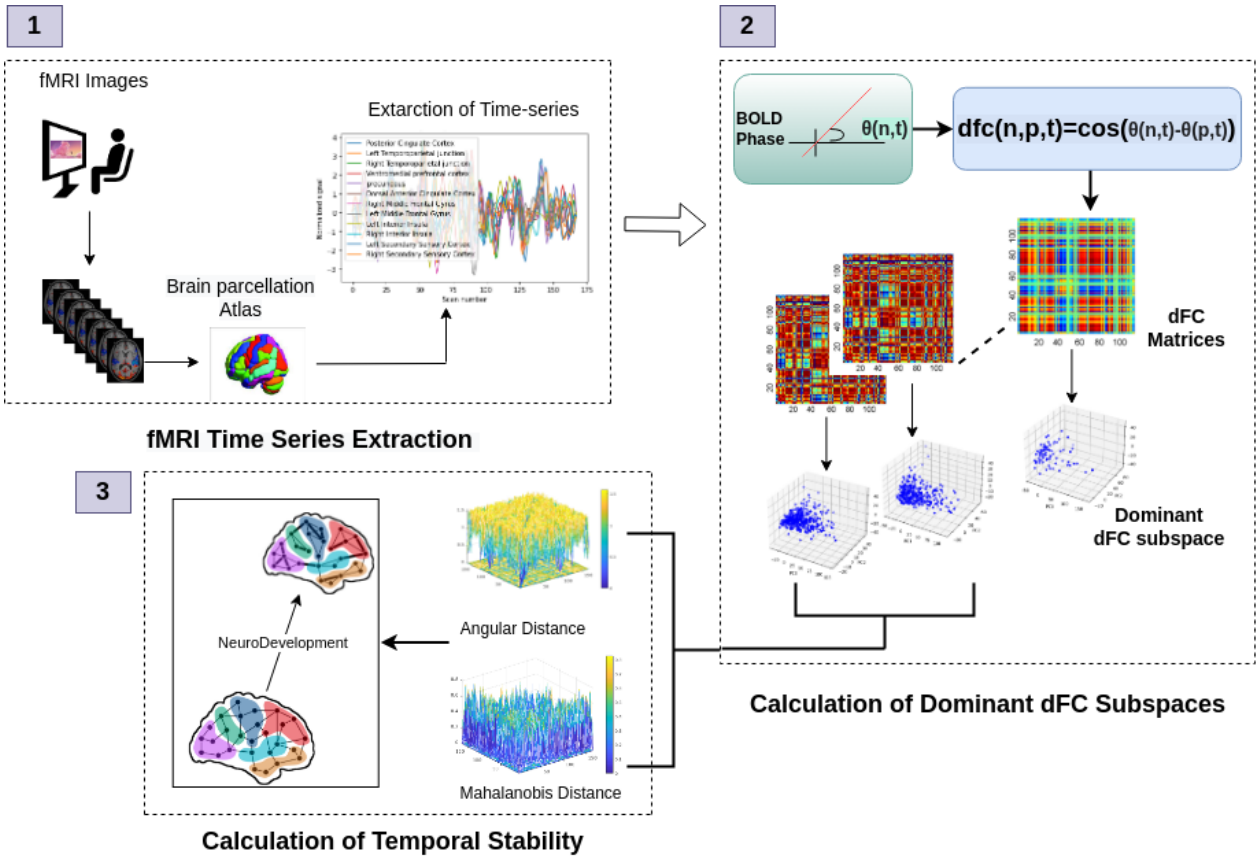

Figure 3.1: Illustrative overview of the proposed unsupervised characterization of dFC of Tom and Pain functional brain networks for identifying critical age where reasonable temporal stability is achieved and, subsequently, how temporal stability patterns predict performance in the false-belief task. The pipeline of the analysis proposed in this work is organized as follows: **1)** Identifying brain regions anchored in ToM and Pain networks and extraction of BOLD fMRI time-series signals from ToM and Pain functional brain regions, **2)** Calculation of Angular distance and Mahalanobis distance using after characterization of dominant dFC subspaces using an unsupervised approach, leading to temporal stability computations, and **3)** Applied auto-regression model to check temporal fluctuations and identifying Markovian process that fully explains the dFC evolution.

coils, 256 mm for adult coils). The whole brain was covered by 32 interleaved near-axial slices that were aligned with the anterior/posterior commissure and and we used a gradient-echo EPI sequence sensitive to BOLD contrast to capture functional data (EPI factor: 64; TR: 2 s, TE: 30 ms, flip angle: 90°) Richardson *et al.* [2018]. All functional data were upsampled in normalized space to 2 mm isotropic voxels. Based on the participant's head motion one TR back, prospective acquisition correction was used to modify the gradient locations.

FMRI data were analyzed using Matlab, R-written custom software, such as SPM8 (`http://www.fil.ion.ucl.ac.uk/spm`) Penny *et al.* [2011]. Every participant's anatomical image was standardized to the Montreal Neurological Institute (MNI) template, and functional images were registered to that image as the first image of the run Cantlon *et al.* [2006]; Burgund *et al.* [2002]. This allowed us to directly compare responses between child and adult participants and utilize group regions of interest (ROIs) and hypothesis spaces generated in adult data sets. Every brain was visually registered to the MNI template, with attention paid to the cortical envelope and interior characteristics such as the main sulci and AC–PC. We smoothed all of the data using a 5 mm kernel Gaussian filter. By use of the ART toolbox (`https://www.nitrc.org/projects/artifact_detect/`) Whitfield-Gabrieli *et al.* [2011], artifact time points were defined as those for which the global signal fluctuated more than three standard deviations from the mean global signal or for which there was >2 mm composite motion relative to the prior time point. If one-third or more of the time points gathered were found to be artifact time points, individuals were removed from the sample. Both the number of artifact time points for the child and adult participants were substantially different (M(s.d.) = 10.5(10.6) for the kid and 2.8(4) for the adult; Welch two-sample t-test: $t(137.7) = 6.49, p < .000001$). The no. of motion artifact timepoints among children did not correlate with either the ToM score (Kendall tau correlation test $(n = 122) : rk(120) = 0.005, p = 0.94$) or the age (spearman correlation test $(n = 122) : rs(120) = 0.02, p = 0.86$). Number of artifact timepoints did not differ between young (3–5 yrs old) children based on falsebelief task performance (linear regression tests for effect of false belief (FB)-Group on number of motion artifact timepoints: NS effect of FB-group (Pass (n = 30) vs. Fail $(n = 15)) : b = 0.04, t = 0.12, p = 0.9$; NS effect of FB-group (Pass (n = 30), Inc (n = 20), or Fail $(n = 15)) : b < 0.05, p > 0.9$) or response inhibition (linear regression test for an effect of Dimensional Change Card Sort task (DCCS) on number of motion artifact timepoints (n = 64): NS effect of DCCS summary score: $b = 0.16, t = 1.18, p = 0.25$). We include number of motion artifact timepoints as a covariate in the analysis even though quantity of motion is matched across children and hence probably not driving developmental effects within the child sample. Mean translation, rotation, and distance metrics are strongly linked (r >.8) with the number of artifact time points.

3.2.2 Explicit ToM Task and False-Belief Composite Score and fMRI Analysis

In the previous study, six explicit ToM-related questions were administered for the false belief task to identify the correlation between brain development and behavioral scores in ToM reasoning across a wide age range of children Richardson *et al.* [2018]. Each child's performance on the ToM-related false belief task was assessed based on the proportion of questions answered correctly out of 24 matched items (14 prediction items and 10 explanation items). Based on the outcome of these explicit false belief task scores, the participants were categorized into three classes: Pass (5-6 correct answers), inconsistent (3-4 correct answers), and fail (0-2 correct answers). In the current study, participants' data were classified in two different ways: (a) into six groups of 3-yrs, 4-yrs, 5-yrs, 7-yrs, 8-12 yrs, and adult age groups (reference), and (b) into three false belief tasks outcome-based groups, i.e., pass, inconsistent, and fail. The classification was undertaken to understand the differential developmental changes in the neural activation patterns Huitt and Hummel [2003]. Due to the unavailability of data on any 6-yrs olds, that age group could not be added to the above categorization. Further, we computed the magnitude of evoked responses to

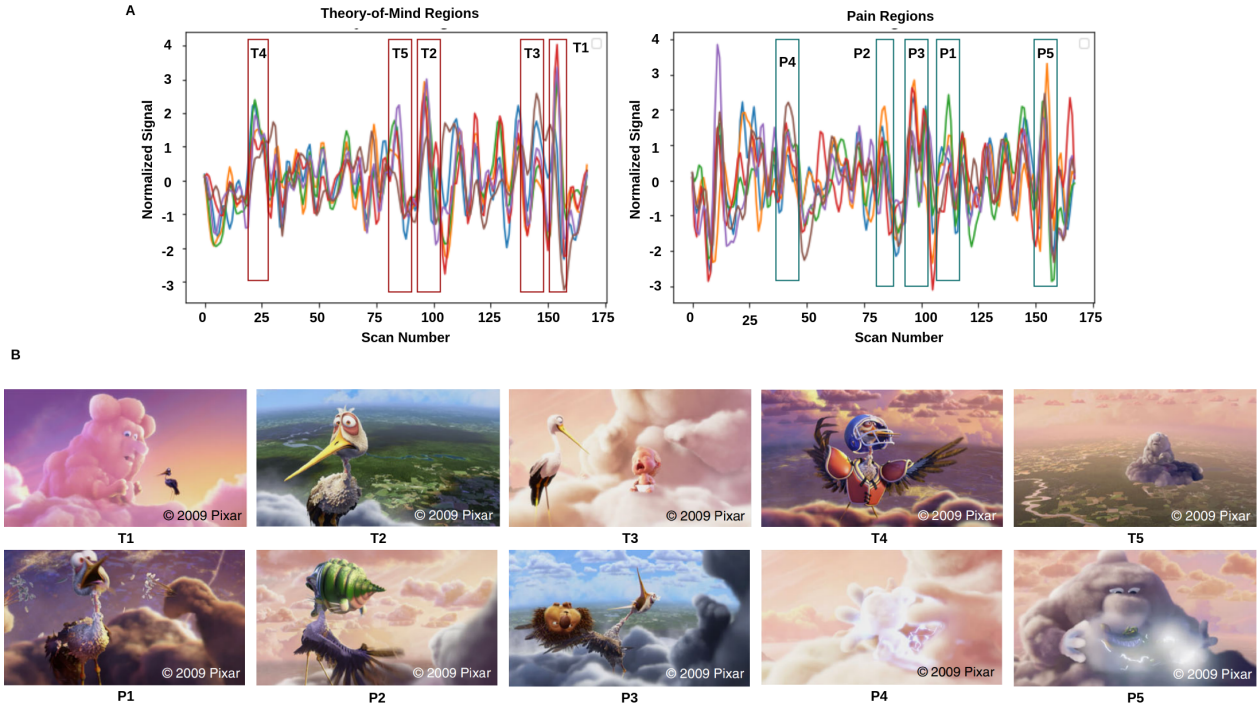

Figure 3.2: Movie demonstration: **A)** response magnitude that evoked maximum activation in ToM and pain networks. **B)** depicts the movie scenes where higher activation occurred. T1, T2, T3, T4, and T5 represent the ToM scenes with higher activation, whereas P1, P2, P3, P4, and P5 show the pain scenes with higher activation.

the events in the movie that evoked peak response magnitude. To map peak response magnitudes onto movie scenes depicting ToM and Pain events, we first identified time points where the highest activation occurred in predefined ToM and Pain ROIs. These peak responses were computed at the group level by averaging across all children within each age cohort, ensuring that the extracted time points represented consistent activation patterns across participants. However, to examine individual variability, we also computed peak responses separately for each child, allowing for within-subject comparisons. We selected five-time courses ($> 5sec$) (total no. of time-points = 168), from each network according to the previous study Richardson *et al.* [2018], of maximum activation in ToM (Time-points with maximum activation = 18-27, 82-90, 92-102, 140-149, 150-159) and Pain networks (time-points with maximum activation = 35-49, 78-85, 88-92, 104-115, 159-168) (total of ten time-courses) (refer to Figure 7.2 and Table 7.2). the BOLD time series for individual subjects from these groups were extracted from regions of interest (ROIs) anchored in two brain networks - Theory-of-Mind and Pain networks (refer to Table 7.1). The regions selected for ToM were - bilateral Temporoparietal Junction (LTPJ and RTPJ), Posterior Cingulate Cortex (PCC), Ventro- and Dorso-medial Prefrontal Cortex (vmPFC and dmPFC), and Precuneus, whereas the Pain network regions consist of - bilateral Middle Frontal Gyrus (LMFG and RMFG), bilateral Interior Insula, and bilateral Secondary Sensory Cortex (LSSC and RSSC) Richardson *et al.* [2018]. These brain regions and their MNI coordinates were selected from published literature (refer to Table 7.1) Mazziotta *et al.* [1995, 2001]. According to the previous study Richardson *et al.* [2018], we selected two brain networks (ToM and pain) and treated them as distinct entities. The ToM network, comprising regions such as the temporoparietal junction (TPJ), precuneus, and medial prefrontal cortex (mPFC), has been consistently linked to social cognition and mental state attribution. Meanwhile, the pain network, including the anterior insula (AI), anterior cingulate cortex (ACC), and ventromedial prefrontal cortex (vmPFC), is primarily associated with processing

nociceptive and affective pain experiences. Although vmPFC contributes to both networks, prior work suggests its role in affective processing is more pronounced in the pain network than in explicit mentalizing tasks. We used the Schaefer atlas for brain parcellation, and by using MNI coordinates, we created a spherical binary mask with a 10 mm radius for all selected ROIs. We extracted time-series for each participant in two ways: a) from ToM and pain networks separately (6 ROIs each (to check within network variability)) and b) from both the networks (12 ROIs (to check between-network variability or mixed effect)). Further analyses were carried out on the extracted time series signals.

Overall, it included six age groups: 3-yrs, 4-yrs, 5-yrs, 7-yrs, 8-12 yrs, and adults, with a total of 155 participants (67 females, 88 males). The dataset was originally collected by Richardson et al. (2018) Richardson *et al.* [2018] and included explicit Theory of Mind (ToM) tasks and a false-belief composite score to assess children's ability to attribute mental states to others. The behavioral assessment consisted of a structured false-belief task, which included six questions evaluating children's ability to predict and explain actions based on others' false beliefs, desires, and expectations. Participants also completed additional ToM-related tasks assessing moral reasoning and social cognition. The fMRI scanning session included a single movie-viewing task (Partly Cloudy), during which participants watched a 5.6-minute animated movie while their brain activity was recorded. Brain activity was analyzed at key time points corresponding to peak activation in the ToM and pain networks, identified based on prior studies and empirical time-course analyses. Children were not scanned repeatedly; each participant underwent a single scanning session.

The ethical approval for participant recruitment, data collection, and initial study procedures was obtained by the original authors from their respective institutional review boards. Since we are conducting a secondary analysis on this dataset, no direct involvement with human participants occurred in this research. The data were used in accordance with institutional and regulatory guidelines for secondary data analysis. Furthermore, all data were anonymized before access, ensuring the confidentiality and privacy of participants.

3.2.3 BOLD Phase Coherence and Estimation of Dynamic Functional Connectivity

Functional connectivity (FC) is a widely used measure of brain connectivity that quantifies the statistical interdependence between pairs of brain regions over time. FC is estimated from Blood Oxygen Level-Dependent (BOLD) fMRI signals among pairs of brain regions Friston *et al.* [1993]; Biswal *et al.* [1995]; Friston [2011]; Gaudet *et al.* [2020]. However, these correlation and covariance measures assume that the time series signal for specific brain regions remains static over time, which significantly limits our understanding of whole brain dynamics associated with neurodevelopment. Further temporal changes could carry distinct and meaningful connectivity patterns over the scan and developmental time scales across brain regions Chang and Glover [2010]; Menon and Krishnamurthy [2019].

Resting-state data and complex naturalistic stimuli have been shown to encode significant variation among functional brain networks over the entire stimulus duration. Hence, dynamic functional connectivity (DFC) patterns across the whole data set can provide a more penetrating view into the activation patterns over the more commonly used static functional connectivity measure Hutchison *et al.* [2013a]. We have chosen BOLD phase coherence as a measure for the computation of DFC to circumvent the temporal resolution issues that arise in the case of the more popularly employed sliding window correlation method, which is limited by the heuristic selection of the window size. Shorter windows include spurious correlations with high variability and low reliability and have a lower statistical significance due to a lesser number of data points, whereas longer windows are capable of eliminating noise-related correlation while failing to capture

ToM Regions			Pain Regions		
Sr. No.	**ROIs**	**MNI- Co-ordinates (X,Y,Z)**	**Sr. No.**	**ROIs**	**MNI- Co-ordinates (X,Y,Z)**
1	Posterior Cingulate Cortex (PCC)	0, -52, 18	1	Right Middle Frontal Gyrus (RMFC)	36, 38, 40
2	Left Temporoparietal Junction (LTPJ)	-46, -68, 32	2	Left Middle Frontal Gyrus (LMFC)	-36, 38, 40
3	Right Temporoparietal Junction (RTPJ)	46, -68, 32	3	Left Interior Insula (LII)	-40, 22, 0
4	Ventromedial Prefrontal Cortex (vmPFC)	4, 48, -4	4	Right Interior Insula (RII)	39, 23, -4
5	Precuneus	0, -49, 40	5	Left Secondary Sensory Cortex (LSSC)	-39, -15, 18
6	Dorsomedial Prefrontal Cortex (dmPFC)	-10, 58, 24	6	Right Secondary Sensory Cortex (RSSC)	39, -15, 18

Table 3.1: Table shows selected ToM and pain brain regions and corresponding MNI coordinated for extracting time-series signal.

ToM Clips Description		Pain Clips Description	
Sr. No.	**Description**	**Sr. No.**	**Description**
T1	Peck flies away to happy cloud	P1	Gus pulls porcupine spines from Peck's head
T2	Peck caught gazing at happy clouds	P2	Alligator biting Peck
T3	Baby crying, then happy	P3	Peck tossing porcupine
T4	Peck dons gear to show why he left	P4	Cloud makes animals (lightning)
T5	Pan from happy clouds to lonely cloud (Gus)	P5	Gus makes alligator (lightning)

Table 3.2: Table showing the selected time-course where higher activation occurred for ToM and pain networks.

significant transient changes in the time series signals Glerean *et al.* [2012]; Hutchison *et al.* [2013b,a]; Preti *et al.* [2017]

Here, we employ BOLD signal phase coherence and quantify the strength of this synchronization while discarding its amplitude. The phase component of the signal sufficiently captures the temporally transient changes, which follows from the observation that two weakly-coupled nonlinear oscillators can synchronize even without any correlation of their amplitudes. Further, phase coherence does not assume stationarity of signals compared to other transformation and coherence-based methods, making this an ideal unsupervised method for characterizing DFC.

Finally, BOLD phase coherence was employed to estimate time-resolved DFC for each subject, resulting in a $N \times N \times T$ matrix (where N = 12 denotes the number of brain regions and T = 168 represents the total number of time points). To compute the BOLD Phase Coherence, the Hilbert transform was utilized to ascertain the instantaneous phases $\theta(n,t)$ of the BOLD time series. The modulated BOLD signal s(t) was then represented analytically using the following equation Sastry *et al.* [2022]:

$$z(t) = z_r(t) + jz_i(t) = s(t) + jHT[s(t)] \tag{3.1}$$

where $HT[*]$ stands for Hilbert Transformation. Using the following formulae, the instantaneous phase $\theta(t)$ was calculated Sastry *et al.* [2022].

$$\theta(t) = \angle z(t) = \arctan\frac{z_i(t)}{z_r(t)} = \arctan\frac{HT[s(t)]}{s(t)} \tag{3.2}$$

DFC (n,p,t) was then calculated for the predetermined brain areas n and p, as follows Sastry *et al.* [2022]:

$$DFC(n,p,t) = \cos(\theta(n,t) - \theta(p,t)) \tag{3.3}$$

3.2.4 Computation of Dominant Dynamic Functional Connectivity Subspaces

Principal Components Analysis (PCA) is a multivariate, unsupervised dimension reduction technique that separates the data into a set of orthogonal principal components, also known as leading eigenvectors, which are then arranged according to how much variation they contribute to the total variance Cabral *et al.* [2017].

A participant-specific $DFC(n,p,t)$ matrix of dimension $N*N$ reflecting the FC between the nth and pth brain regions at each time point was subjected to principal component analysis (PCA). As a result, $DFC(n,p,t)$ or simply DFC_t may be written as:

$$DFC_t = V^T SV \tag{3.4}$$

Where S stands for the diagonal matrix, and V stands for the leading eigenvector of the $N \times N$ matrix:

$$\begin{bmatrix} \lambda_1 & \cdots & 0 \\ \vdots & \ddots & \vdots \\ 0 & \cdots & \lambda_N \end{bmatrix}, \quad \text{such that } \lambda_1 > \lambda_2 > \cdots > \lambda_N.$$

The primary components of the DFC are represented by the number of $k = 3$. The dominating DFC $D(n,k,t)$ was calculated as follows:

$$D = \tilde{V}^T \tilde{S} \tilde{V} \tag{3.5}$$

where dimensionally reduced matrix is denoted by $\tilde{V}^T$ and $\tilde{S}$ is representing diagonal matrix $\begin{bmatrix} \lambda_1 & \cdots & 0 \\ \vdots & \ddots & \vdots \\ 0 & \cdots & \lambda_N \end{bmatrix}$. Here, we choose k=3 or three leading eigenvectors that contain 85% information.

3.2.5 Computation of Network Temporal Stability using Dominant dFC Subspaces

We characterize the temporal stability of dominant DFC subspaces by estimating their similarity between different time points throughout. Additionally, quantifying the temporal stability of a network over the period of data acquisition can also vouch for the reliability of the connectivity observed and the robustness of the network activity in the face of external disturbances. We used two techniques to achieve that goal: Mahalanobis distance and Angular distance. We used the following equation to determine the distance between DFC sub-spaces from different time points Sastry *et al.* [2022]:

1. **Angular Distance Calculation:** Angular distance measures the angle between two vectors or subspaces, which in this study represent dynamic functional connectivity (DFC) patterns at different time points. The angular distance $\phi(t_x, t_y)$ between two DFC subspaces D_{t_x} and D_{t_y} is calculated using the following equation:

$$\phi(t_x, t_y) = \angle(D_{t_x}, D_{t_y}) \tag{3.6}$$

   Here, each entry of the temporal stability matrix $\phi(t_x, t_y)$ represents the angular separation between the dominant DFC subspaces at time points t_x and t_y. The angular distance ranges from 0 to $\frac{\pi}{2}$, where $\frac{\pi}{2}$ denotes high angular distance and 0 denotes low angular distance. D_{t_x} and D_{t_y} are matrices of dimensions $R \times 2$, where R represents the number of regions of interest (ROIs) in the brain.

2. **Mahalanobis Distance Calculation:** We estimated the Euclidean distance using the Mahalanobis distance method, which measures the distance between distinct points from one space to another. This was performed for each participant's DFC dominating subspace using the following equation:

$$M^2 = (D_{t_x} - D_{t_y})^T C^{-1} (D_{t_x} - D_{t_y}) \tag{3.7}$$

   Here, M^2 represents the distance between each point. In this equation, C denotes the covariance matrix, which characterizes the variability and relationships between different dimensions of the data. By taking the inverse of C (C^{-1}), we normalize the distances based on the covariance structure of the data. The resulting Mahalanobis distance matrix provides a measure of similarity between DFC subspaces at different time points.

Basically, Angular distance was employed to quantify within-subject variability by measuring the difference in DFC subspaces across different time points within an individual. Higher Angular distance values indicate greater fluctuations in dynamic connectivity, reflecting less stable functional interactions. This is particularly crucial in developmental studies, as shorter-lived connectivity states in younger children may signify an ongoing maturation process. On the other hand, Mahalanobis distance was used to assess between-subject variability by capturing how distinct an individual's connectivity pattern is compared to the mean pattern of their age cohort. This distance metric accounts for variance and correlations within the dataset, making it a robust measure for evaluating deviations in connectivity stability. Applying both metrics allows us to discern age-related trends in functional network stability and provides insights into how DFC variability correlates with neurodevelopmental trajectories.

3.2.6 Validation of Results

1. **Entropy:** To validate results of temporal stability matrices, we calculated entropy that defined measurement of detectable temporal order that we may interpret as the overall stability of the temporal stability matrices Sastry *et al.* [2022]. The lower the value of entropy, the higher the instability in the temporal patterns and vice versa. For each subject, we compute the entropy of temporal stability matrices, where each element is the estimated Mahalanobis or Angular distance between the dominant subspaces D_{t_x} and D_{t_y}. The entropy was calculated using following formula Sastry *et al.* [2022]:

$$E = -\Sigma plog(p) \tag{3.8}$$

   Where, p holds the normalized histogram counts.

2. **Frobenius norm:** Frobenius norm or Euclidean norm of matrix was utilized to quantify the variations between the temporal stability matrices generated for different age groups. We calculated Frobenius norm using following formula Sastry *et al.* [2022]:

$$\| x_F \| = \sqrt{\Sigma_{i=1}^{T} \Sigma_{j=1}^{T} |a_{ij} - b_{ij}|^2} \tag{3.9}$$

   Where entries of temporal matrices are indicated by a_{ij} and b_{ij}.

3.2.7 Stochastic Characterization of dFC

The degree of temporal changes in functional networks captured within the observed temporal fluctuations can be identified by using the principal angle and the Mahalanobis distance between the dominent dFC subspaces Sastry *et al.* [2022]. We make use of auto-regressive (AR) models to uncover the underlying stochastic properties of these measurements (Refer to Figure 1). $AR(\rho)$ concept was implemented using following equation Sastry *et al.* [2022]:

$$X_t = c + \Sigma_{i=1}^{\rho} \varphi_i X_{t-i} + \varepsilon_t \tag{3.10}$$

Where $\varphi_1 ..... \varphi_\rho$ =parameters of model, c= constant, ε_t = white noise, ρ = model order Sastry *et al.* [2022]. The Akaike information criterion may be used to calculate the ideal model of an AR process (AIC) using following equation Sastry *et al.* [2022]:

$$AIC(\rho) = -2L + 2\rho \tag{3.11}$$

Where L is the likelihood function. We estimated several values for the model order parameter $AR(\rho)$, ranging from 0 to 100, and then chose the AR model with the first minimum AIC score

Dieter *et al.* [2016]; Sastry *et al.* [2022]; Akaike [1974]. If it is determined that the model order is larger than 1, the underlying process is regarded as being non-Markovian.

3.3 RESULTS

To assess the developmental trajectory of stability in ToM and Pain networks, we computed angular distance and Mahalanobis distance across six age subgroups. We employed two approaches: one considering all 12 ROIs together and another analyzing ToM and Pain networks separately. Results indicated a general trend of decreasing angular distance and increasing network stability from early childhood to adulthood. Notably, 4-year-olds and 7-year-olds exhibited anomalously higher angular distances, indicating transient instability in functional coordination. In contrast, the 5-year-olds displayed a stability pattern more similar to the 8-12 years group, suggesting an early transition toward mature network dynamics. These findings align with prior studies showing that neural networks undergo non-linear transitions during early development, likely reflecting synaptic pruning and refinement of functional connectivity . The increasing stability of higher-order cognitive regions within the ToM and Pain networks may enhance adaptability and integrative processing, supporting more efficient social and sensory-cognitive interactions.

3.3.1 Distinct Temporal Stability of ToM and Pain Network in 3-12 years age

1. **Computation of Temporal Stability using Angular Distance:** To check the distinct temporal stability of ToM and Pain networks at 3-12 yrs of age, we first calculated angular distance matrices among dominant DFC subspaces identified over all the time points. Subsequently, a $time * time$ temporal stability matrix was derived, which was then averaged over all individuals. Each entry in the matrix represented the angle between the dominating DFC subspaces at t_x and t_y. As described earlier, we calculated Angular distance into two parts: one for six age categories (3-yrs to adults) and one for the three false-belief-task performance groups. Figures 7.3 and 7.4 represent the subject-average temporal matrices for all 12 ROIs and 6 ROIs in each ToM and Pain network. The higher the value of angular distance, the bigger the leap between two dominant DFC subspaces at time points t_x and t_y. Our results suggested that in terms of capturing temporal stability for defined time courses (For the ToM network (Time-points with maximum activation = 18-27, 82-90, 92-102, 140-149, 150-159) and for pain networks (time-points with maximum activation =35-49, 78-85, 88-92, 104-115, 159-168) (total of ten time courses)) for all ROIs or, in other words, variability between the networks, we were getting shorter-lived repeated patterns of temporal stability for 3-yrs and 4-yrs age groups. Whereas, for other age groups, i.e., 5-yrs, 7-yrs, 8-12 yrs, and adults, we were getting longer-lived temporal stability patterns for defined time courses (refer to Figure 7.3). The previous study Richardson *et al.* [2018] reported that ToM network segregated as early as 3-yrs from pain network. To get more insight, we also calculated temporal stability for ToM and pain network separately to check variability within the network. We found longer-lived temporal stability patterns for defined time courses in the ToM network, even for 3-yrs and 4-yrs age groups, and it continued till adulthood. Whereas we observed shorter-lived repeated patterns of temporal stability for 3-yrs and 4-yrs age groups in pain network and found change in the pattern from 5-yr age group (i.e., longer-lived stability pattern) that continued till adulthood. The temporal matrices per age group show higher distance values for All ROIs than the corresponding matrices for ToM or Pain ROIs, and this difference persists through age (refer to Figures 7.3, 7.4, and 7.5).

To quantify differences between temporal matrices, the distance values were converted into Z-scores, and Kolmogorov-Smirnov tests for equality of distributions (all groups were found to have unequal distributions with p varying from < 0.4 to $< 4 \times 10^{-313}$), followed by Kruskal Wallis tests were conducted: All ROIs $\chi^2(5) = 42.04$, $p < 6 \times 10^{-8}$; Pain ROIs $\chi^2(5) = 47.63$, $p < 5 \times 10^{-9}$; ToM ROIs $\chi^2(5) = 24.59$, $p < 0.0003$. Dunn-Sidak post-hoc test was performed for pairwise comparisons: All ROIs: 3yrs-4yrs: diff=-1376.4, $p = 0.0114$, 4yrs-5yrs: diff=1716.9, $p = 4.8131 \times 10^{-4}$, 4yrs-8yrs: diff=2212.4, $p = 1.3683 \times 10^{-6}$, 4yrs-Adult: diff=2004.2, $p = 1.9045 \times 10^{-5}$, 7yrs-8-12yrs: diff=1551.7, $p = 0.0025$, 7yrs-Adult: diff= 1343.6, $p = 0.0149$; Pain ROIs: 3yrs-8-12yrs: diff= 1365.7, $p = 0.0125$, 3yrs-Adult: diff=1196.6, $p = 0.0445$, 4yrs-5yrs: diff=1735.3, $p = 3.9715 \times 10^{-4}$, 4yrs-8-12yrs: diff=2337.3, $p = 2.6373 \times 10^{-7}$, 4yrs-Adult: diff=2168.2, $p = 2.4350 \times 10^{-6}$, 7yrs-8-12yrs: diff=1556.7, $p = 0.0023$, 7yrs-Adult: diff=1387.6, $p = 0.0104$; ToM ROIs: 3yrs-8-12yrs: diff=1286.6, $p = 0.0232$, 4yrs-8-12yrs: diff=1836.4, $p = 1.3342 \times 10^{-4}$, 4yrs-Adult: diff=1319.2, $p = 0.0180$, 7yrs-8-12yrs: diff=1302.9, $p = 0.0205$; rest NS.

Entropy was calculated to quantify the complexity of these temporal stability patterns. Figure 7.5 shows the entropy values calculated from angular distance values for the six age groups as violin plots. In all three graphs (Figure 7.5 subgraphs - A, E, F), a higher entropy value is noticed for 4 yrs compared to the other age groups. A lower entropy value is noticed for 7 yrs group as compared to the 5 yrs group, and this corroborates with the qualitative conclusions drawn from the temporal matrices earlier. Kolmogorov-Smirnov test was performed to check for equality of distributions (all groups were found to have unequal distributions with $p < 0.05$), followed by the Kruskal-Wallis tests with non-significant results at 5% confidence level (All ROIs $\chi^2(5) = 5.54$, $p < 0.4$; Pain ROIs $\chi^2(5) = 10.97$, $p < 0.06$; ToM ROIs $\chi^2(5) = 4.13$, $p < 0.6$).

In addition, we computed the Frobenius distance to examine the difference among temporal matrices of ToM and Pain regions (Figure 4). We find Frobenius distance values to progressively reduce from 3 yrs to Adults, with an anomalous dip for 5 yrs. No statistical significance was found using the Kruskal-Wallis test ($\chi^2(5) = 7.59$, $p < 0.2$).

2. **Computation of Temporal Stability using Mahalanobis Distance:** Next, we estimated the Mahalanobis distance to assess the temporal stability of the dFC. Each matrix element represents the Mahalanobis distance between the dominating dFC subspaces. A higher value of Mahalanobis Distance denotes a larger distance between the average of the Euclidean distance between individual ROIs at t_x and the collection of all ROIs (ToM or Pain network ROIs) at t_y of the dominant dFC subspaces. The above can be interpreted similarly to the Angular Distance measure. We observe a trend of decreasing high distance values to lower overall distance values from children to adults. Consistent with the previous measure, we also find a slight increase in temporal switching dynamics from 5 yrs to 7 yrs and an increase in distance values from 3 yrs to 4 yrs. A major reason for the limited inference drawn from these graphs is the presence of outlying data points with high distance values, which obscures smaller distance values.

   Z-scores were calculated to compare the temporal matrices of these subgroups, Kolmogorov-Smirnov test was performed (all groups were found to have unequal distributions with p varying from $< 2 \times 10^{-8} to < 1 \times 10^{-255}$), followed by Kruskal-Wallis(All ROIs $\chi^2(5) = 18066.11$, $p = 0$; Pain ROIs $\chi^2(5) = 3863.9$, $p = 0$; ToM ROIs $\chi^2(5) = 5254.75$, $p = 0$) and Dunn-Sidak tests (Refer to Table 3).

   To validate the results, we calculated entropy (shown in Figure 5), with similar entropy values seen across the age groups, with an exception for ToM ROIs, which displays a

Pairs	All ROIs		Pain ROIs		ToM ROIs	
	Diff.	p-value	Difference	p-value	Difference	p-value
3yrs-4yrs	53917	$\mathbf{2.0676 \times 10^{-8}}$	4719.4	$\mathbf{2.0172 \times 10^{-8}}$	23518	$\mathbf{2.0693 \times 10^{-8}}$
3yrs-5yrs	31162	$\mathbf{2.1276 \times 10^{-8}}$	−16415	$\mathbf{2.0914 \times 10^{-8}}$	−1104.3	0.0818
3yrs-7yrs	18966	$\mathbf{1.0264 \times 10^{-8}}$	−8762	$\mathbf{2.0472 \times 10^{-8}}$	8240.2	$\mathbf{2.0216 \times 10^{-8}}$
3yrs-8-12yrs	24470	$\mathbf{2.0676 \times 10^{-8}}$	−9564.9	$\mathbf{1.9824 \times 10^{-8}}$	−1192.5	0.0458
3yrs-Adult	29884	$\mathbf{2.7153 \times 10^{-8}}$	−13855	$\mathbf{2.9648 \times 10^{-8}}$	6363.1	$\mathbf{3.5734 \times 10^{-8}}$
4yrs-5yrs	−22755	$\mathbf{2.7859 \times 10^{-8}}$	−21135	$\mathbf{4.6713 \times 10^{-8}}$	−24623	$\mathbf{2.8327 \times 10^{-8}}$
4yrs-7yrs	−34951	$\mathbf{1.4892 \times 10^{-8}}$	−13481	$\mathbf{2.7937 \times 10^{-8}}$	−15278	$\mathbf{2.6153 \times 10^{-8}}$
4yrs-8-12yrs	−29447	$\mathbf{2.5376 \times 10^{-8}}$	−14284	$\mathbf{1.6473 \times 10^{-8}}$	−24711	$\mathbf{3.9347 \times 10^{-8}}$
4yrs-Adult	−24033	$\mathbf{2.0163 \times 10^{-8}}$	−18574	$\mathbf{2.0672 \times 10^{-8}}$	−17155	$\mathbf{2.0748 \times 10^{-8}}$
5yrs-7yrs	−12197	$\mathbf{3.9475 \times 10^{-8}}$	7653.3	$\mathbf{3.0121 \times 10^{-8}}$	9344.4	$\mathbf{1.8392 \times 10^{-8}}$
5yrs-8-12yrs	−6692	$\mathbf{2.0947 \times 10^{-8}}$	6850.4	$\mathbf{2.0134 \times 10^{-8}}$	−88.2839	0.9999
5yrs-Adult	−1278	0.0247	2560.7	$\mathbf{2.9612 \times 10^{-8}}$	7467.4	$\mathbf{2.0632 \times 10^{-8}}$
7yrs-8-12yrs	5504.7	$\mathbf{2.6478 \times 10^{-8}}$	−802.8698	0.3779	−9432.7	$\mathbf{1.9365 \times 10^{-8}}$
7yrs-Adult	10919	$\mathbf{3.9574 \times 10^{-8}}$	−5092.6	$\mathbf{1.5384 \times 10^{-8}}$	−1877	$\mathbf{8.4552 \times 10^{-5}}$
8-12yrs-Adult	5414.1	$\mathbf{5.0253 \times 10^{-8}}$	−4289.7	$\mathbf{2.7346 \times 10^{-8}}$	7555.7	$\mathbf{1.8345 \times 10^{-8}}$
Pass-Inc	11114	$\mathbf{9.5606 \times 10^{-10}}$	-	-	10777	$\mathbf{9.8573 \times 10^{-10}}$
Pass-Fail	2515.5	$\mathbf{7.7497 \times 10^{-10}}$	-	-	13537	$\mathbf{5.8576 \times 10^{-10}}$
Inc-Fail	−8598.4	$\mathbf{8.8746 \times 10^{-10}}$	-	-	2759.2	$\mathbf{6.8475 \times 10^{-10}}$

Table 3.3: Table with difference and p-values calculated using the post-hoc pair-wise Dunn-Sidak test for Mahalanobis Distance-derived Z-scores for the six age subgroups (3, 4, 5, 7, 8-12 yrs and Adult), and for the False-Belief Performance results

Pairs	Angular Distance			Mahalanobis Distance		
	All ROIs	Pain ROIs	ToM ROIs	All ROIs	Pain ROIs	ToM ROIs
3-5 vs 7-12	0.2251	0.5430	0.4079	0.2711	0.7853	**0.0458**
7-12 vs Adult	0.9614	0.2617	0.2463	0.9311	0.4886	0.9080
3-5 vs Adult	0.2794	**0.0443**	0.8361	0.2043	0.8029	0.0691

Table 3.4: Table with p-values calculated for Kolmogorov-Smirnov test between three (3-5, 7-12 year olds, and Adult) age groups of subjects, for Angular and Mahalanobis Distance entropy values.

pattern similar to the observations from the angular distance measure: a higher entropy (and hence more complexity) in 4 yrs as compared to 3 yrs, and in 7 yrs as compared to 5yrs. Kolmogorov-Smirnov test was performed to check for equality of distributions (all groups were found to have unequal distributions with $p < 0.05$), followed by the Kruskal Wallis tests (All ROIs $\chi^2(5) = 72.57$, $p < 3 \times 10^{-14}$; Pain ROIs $\chi^2(5) = 77.87$, $p < 2.5 \times 10^{-15}$; ToM ROIs $\chi^2(5) = 82.44$, $p < 3 \times 10^{-16}$) and Dunn-Sidak for the significant results of the six age subgroups (All ROIs: 3yrs-Adult: diff=-82.5009, $p = 3.1472 \times 10^{-8}$, 4yrs-Adult: diff=-72.7089, $p = 5.6670 \times 10^{-6}$, 5yrs-Adult: diff=-77.3391, $p = 2.0698 \times 10^{-8}$, 7yrs-Adult: diff=-76.595, $p = 2.5474 \times 10^{-8}$, 8-12yrs-Adult: diff=-64.2068, $p = 9.1637 \times 10^{-8}$; Pain ROIs: 3yrs-Adult: diff=-77.9412, $p = 1.0955 \times 10^{-7}$, 4yrs-Adult: diff=-76.0714, $p = 1.6206 \times 10^{-6}$, 5yrs-Adult: diff=-81.3824, $p = 2.0677 \times 10^{-8}$, 7yrs-Adult: diff=-77.0435, $p = 2.4449 \times 10-8$, 8-12yrs-adult: diff=-74.2941, $p = 2.0845 \times 10^{-8}$; ToM ROIs: 3yrs-Adult: diff=-77.1301, $p = 1.4829 \times 10^{-7}$, 4yrs-Adult: diff=-75.5671, $p = 1.9607 \times 10^{-6}$, 5yrs-Adult: diff=-83.0419, $p = 2.0676 \times 10^{-8}$, 7yrs-Adult: diff=-58.8590, $p = 2.0455 \times 10^{-5}$, 8-12yrs-Adult: diff=064.6889, $p = 7.5010 \times 10^{-8}$;

Pairs	Angular Distance			Mahalanobis Distance		
	All ROIs	**Pain ROIs**	**ToM ROIs**	**All ROIs**	**Pain ROIs**	**ToM ROIs**
3 vs 4	0.3775	0.4116	0.8429	0.5841	0.9752	0.9308
3 vs 5	0.4993	0.6701	0.9516	0.3507	0.1496	0.9516
3 vs 7	0.2994	0.3399	0.5761	0.1916	0.3092	0.2994
3 vs 8-12	0.4993	0.6701	0.4993	0.1496	0.9516	0.3507
3 vs Adult	0.5455	0.0686	0.8733	0.0686	0.6916	0.4205
4 vs 5	**0.0494**	0.2705	0.9023	0.4916	0.6512	0.5357
4 vs 7	**0.0160**	0.1853	0.7038	0.8401	0.9892	0.2275
4 vs 8-12	0.0822	0.1803	0.1915	0.6979	0.9436	0.2419
4 vs Adult	**0.0306**	**0.0293**	0.6789	0.7839	0.8571	0.0995
5 vs 7	0.6454	0.9351	0.6288	0.8937	0.8561	**0.0469**
5 vs 8-12	0.8253	0.9624	0.4223	0.4223	0.2650	0.1553
5 vs Adult	0.8919	0.2234	0.9850	0.6495	0.5487	0.1841
7 vs 8-12	0.9554	0.8755	0.3509	0.1464	0.6454	0.9395
7 vs Adult	0.7980	0.3164	0.5317	0.2444	0.6236	0.7902
8-12 vs Adult	0.9714	0.3296	0.0594	0.7685	0.6368	0.9671

Table 3.5: Table with p-values calculated for Kolmogorov-Smirnov test between six (3, 4, 5, 7, 8-12 year olds, and Adult) age groups of subjects, for Angular and Mahalanobis Distance entropy values.

rest NS) (Refer to Table 3.5).

We also calculated the Frobenius distance between the ToM and Pain network ROIs for the six age subgroups (Refer to Figure 7.5). We observe a higher distance for 3 yrs and Adults and a lower distance for all the other age groups. No statistical significance was found using the Kruskal-Wallis test ($\chi^2(5) = 7.78$, $p < 0.2$).

3. **Stochastic Characterization of Temporal Stability Measures:** We investigated the stochastic characteristics of dFC development by using the principal angle $\phi(t)$ and Mahalanobis distance M(t) as time functions. The temporal changes in $\phi(t)$ and M(t) are defined as autoregressive processes to yield the function: $AR(\rho)$. Further, the first minimum AIC score for the generated AR models is considered the best-fit model order. We found the optimum model order of $\rho \geq 2$ for Angular distance and $\rho \geq 4$ for Mahalanobis distance.

3.3.2 Association between Performance in false belief task and Temporal Stability of DFC

Next, we tested our hypothesis that the temporal stability patterns of social brain regions of ToM in 3-12 yrs could be associated with behavioral scores of the false belief task. Temporal instability was a dominant feature at 3 and 4 yrs, but at age 5, we discovered higher temporal stability. We regressed out the age factor and calculated temporal stability for false belief task-based groups. In the current dataset, out of 65 participants (age ranges 3-5 yrs), 15 participants failed the false belief task. They belonged to 3 yrs and 4 yrs age groups, whereas 20 participants were inconsistent during tasks and belonged to mostly 3 yrs and 4 yrs and few participants from 5 yrs. 30 participants passed the task till age 5-yrs. Approximately all participants passed the task from 5 yrs age group onward. In our analysis, we focused on children aged 3-5 yrs for the false-belief task performance, as this age range exhibits significant variability in passing, failing, or inconsistent results. It allows us to

Pairs	Angular Distance	Mahalanobis Distance
3 vs 4	0.3149	0.4848
3 vs 5	0.0300	0.4993
3 vs 7	0.0496	0.9834
3 vs 8-12	0.0300	0.4993
3 vs Adult	0.0116	0.3605
4 vs 5	0.2559	0.8859
4 vs 7	0.4963	0.7038
4 vs 8-12	0.2419	0.3179
4 vs Adult	0.3222	0.5832
5 vs 7	0.5073	0.6371
5 vs 8-12	0.4223	0.4223
5 vs Adult	0.7192	0.4370
7 vs 8-12	0.4541	0.7836
7 vs Adult	0.6151	0.9226
8-12 vs Adult	0.6813	0.2097
3-5 vs 7-12	0.1675	0.2458
7-12 vs Adult	0.0708	0.2288
3-5 vs Adult	0.8620	0.4541

Table 3.6: Table with p-values calculated for Kolmogorov-Smirnov test for three (3-5, 7-12 year olds, and Adult) and six (3, 4, 5, 7, 8-12, and Adult) age group subjects, Frobenius Distance between TOM and Pain Angular and Mahalanobis Distances.

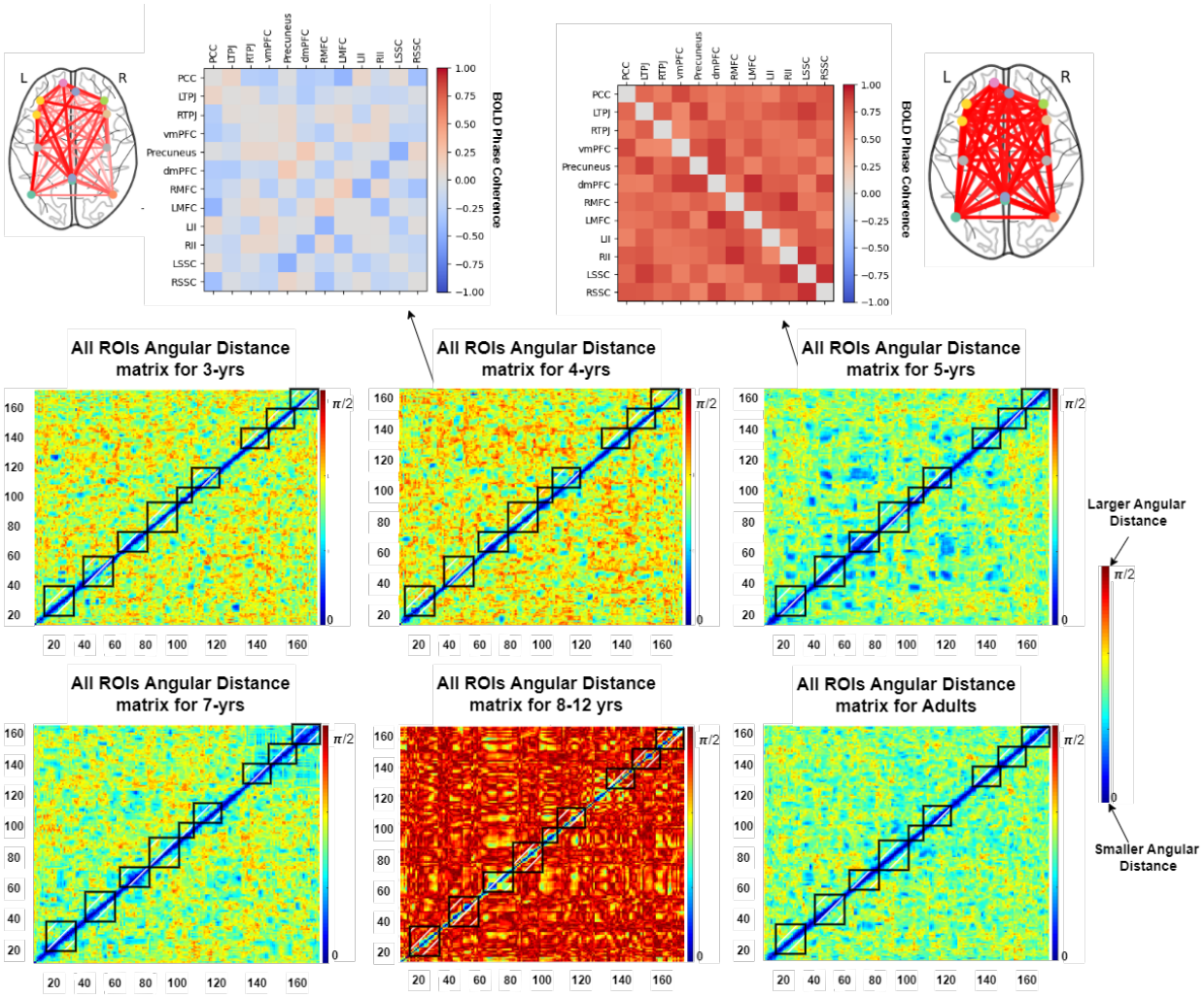

Figure 3.3: Angular distance matrices depicting temporal patterns of all ROIs of the ToM and Pain networks for six age groups (3-yrs, 4-yrs, 5-yrs, 7-yrs, 8-12 yrs children and Adults). Each entry in the matrix represents principal angle $\phi(t_x, t_y)$ between dominant DFC subspaces t_x and t_y that varies from 0 (lower angular distance) to $\pi/2$ (higher angular distance). 3-yrs and 4-yrs age groups showed shorter-lived patterns of temporal stability, whereas 5-yrs, 7-yrs, 8-12 yrs, and adults showed longer-lived patterns of temporal stability for defined time-courses.

Angular Distance			Mahalanobis Distance		
All ROIs			**All ROIs**		
	AIC	**MO**		**AIC**	**MO**
3 yrs	−461.39	5	**3 yrs**	−1550.3	4
4 yrs	−360.21	6	**4 yrs**	−1349.6	4
5 yrs	−508.79	2	**5 yrs**	−1535.1	5
7 yrs	−488.25	5	**7 yrs**	−1525.4	4
8-12 yrs	98.69	6	**8-12 yrs**	−944.94	11
Adult	−502.03	4	**Adult**	−1440.6	4
Pain ROIs			**Pain ROIs**		
	AIC	**MO**		**AIC**	**MO**
3 yrs	−494.14	5	**3 yrs**	−1506.8	4
4 yrs	−455.69	8	**4 yrs**	−1516.4	4
5 yrs	−493.04	6	**5 yrs**	−1461.9	4
7 yrs	−513.25	4	**7 yrs**	−1353.5	10
8-12 yrs	−613.47	5	**8-12 yrs**	−1349.4	4
Adult	−632.96	6	**Adult**	−1815.1	4
ToM ROIs			**ToM ROIs**		
	AIC	**MO**		**AIC**	**MO**
3 yrs	−584.51	4	**3 yrs**	−1743.5	4
4 yrs	−485.89	5	**4 yrs**	−467.01	4
5 yrs	−595.74	4	**5 yrs**	−1785.2	5
7 yrs	−615.09	8	**7 yrs**	−1391.5	4
8-12 yrs	−442.53	6	**8-12 yrs**	−1771.7	11
Adult	−480.73	2	**Adult**	−1322.6	8

Table 3.7: Table with (the first) minimal AIC score and the corresponding Model Order number, obtained for the stochastic characterization of the Angular and Mahalanobis Distance temporal matrices for 6 age groups (3, 4, 5, 7, 8-12, and Adult) of subjects

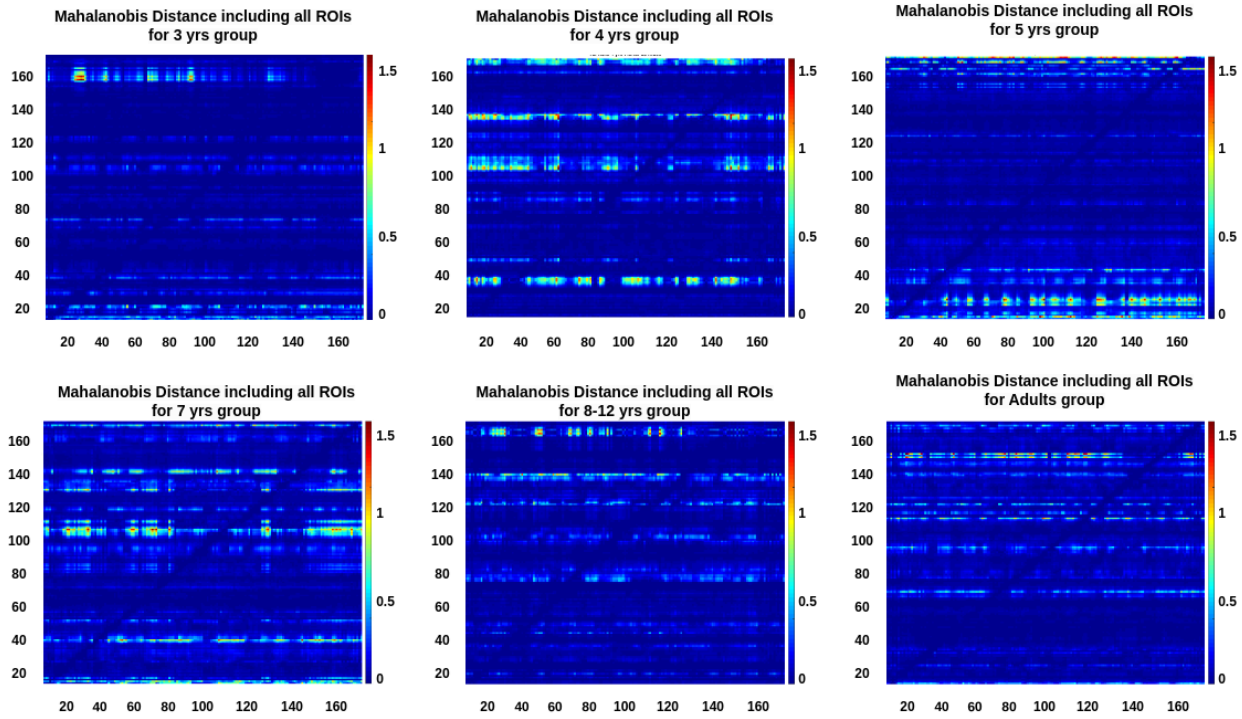

Figure 3.4: Mahalanobis distance matrices depicting temporal patterns of all ROIs of the ToM and Pain networks for six age groups (3, 4, 5, 7,8-12-year children and Adults) that show low dimension pattern high dimensionality functional connectivity.

Angular Distance			**Mahalanobis Distance**		
All ROIs			**All ROIs**		
	AIC	**MO**		**AIC**	**MO**
3-5 yrs	39.8347	8	**3-5 yrs**	-1512.8	4
7-12 yrs	98.6944	6	**7-12 yrs**	-1010.9	14
Adult	-502.0290	4	**Adult**	-1400.6	4
Pain ROIs			**Pain ROIs**		
	AIC	**MO**		**AIC**	**MO**
3-5 yrs	-647.5301	8	**3-5 yrs**	-1489.2	4
7-12 yrs	-626.9163	4	**7-12 yrs**	-1275.9	11
Adult	-632.9611	6	**Adult**	-1815.1	4
ToM ROIs			**ToM ROIs**		
	AIC	**MO**		**AIC**	**MO**
3-5 yrs	-678.4673	5	**3-5 yrs**	-1432.6	4
7-12 yrs	-695.6764	8	**7-12 yrs**	-1765.5	11
Adult	-480.7293	2	**Adult**	-1322.6	8

Table 3.8: Table with (the first) minimal AIC score and the corresponding Model Order number, obtained for the stochastic characterization of the Angular and Mahalanobis Distance temporal matrices for three age group (3-5, 7-12 year olds and Adult) subjects.

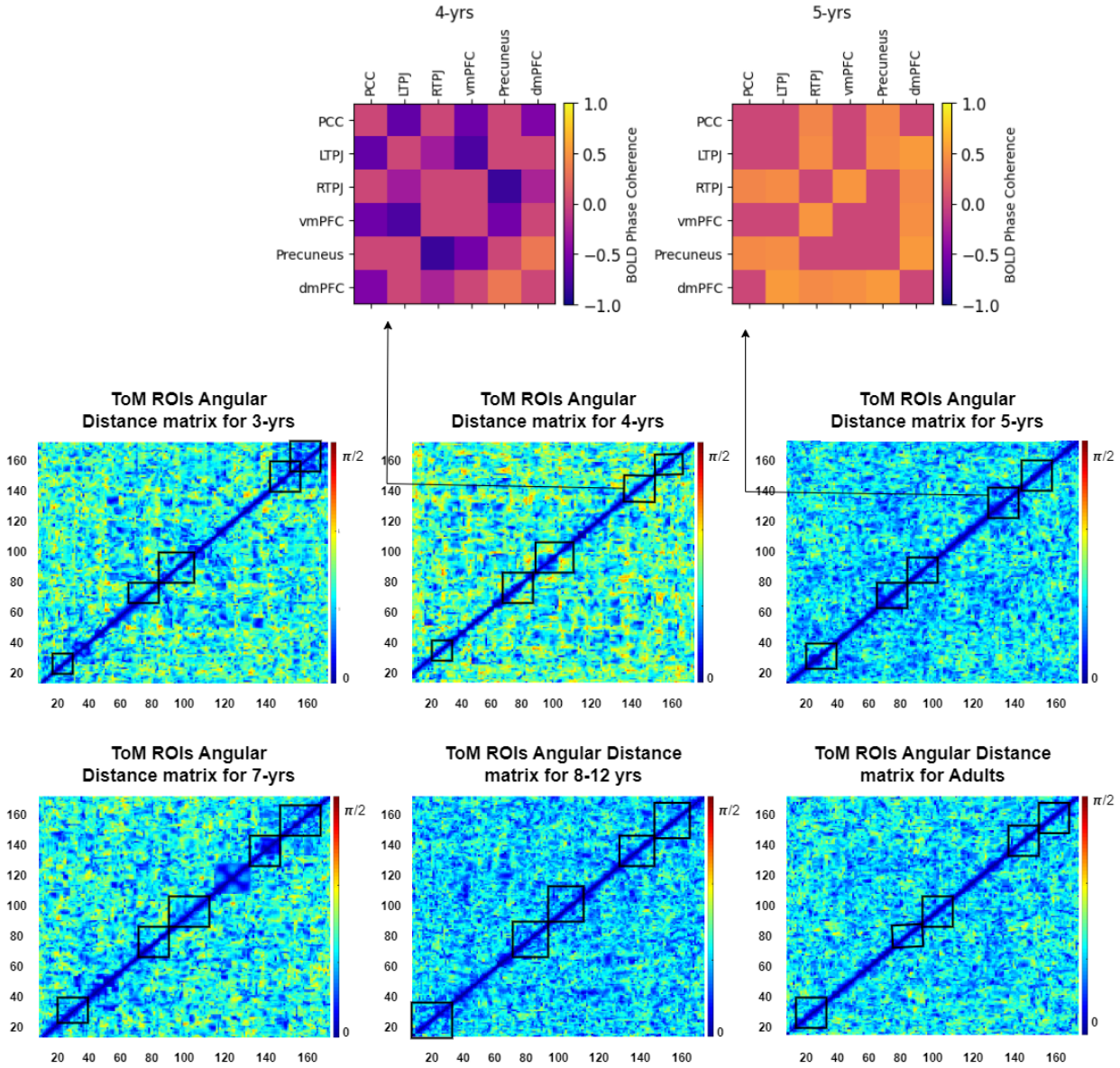

Figure 3.5: Angular distance matrices depicting temporal patterns of ToM network ROIs for each of the six age groups (3, 4, 5, 7, 8-12 yrs and Adults age groups). Earlier, we defined Time-points with maximum activation in ToM network = 18-27, 82-90, 92-102, 140-149, 150-159. We observed longer-lived local spread temporal stability patterns for defined time courses in the ToM network for 5-yrs to adulthood. Whereas we found shorter-lived repeated patterns of temporal stability for 3-yrs and 4-yrs age groups.

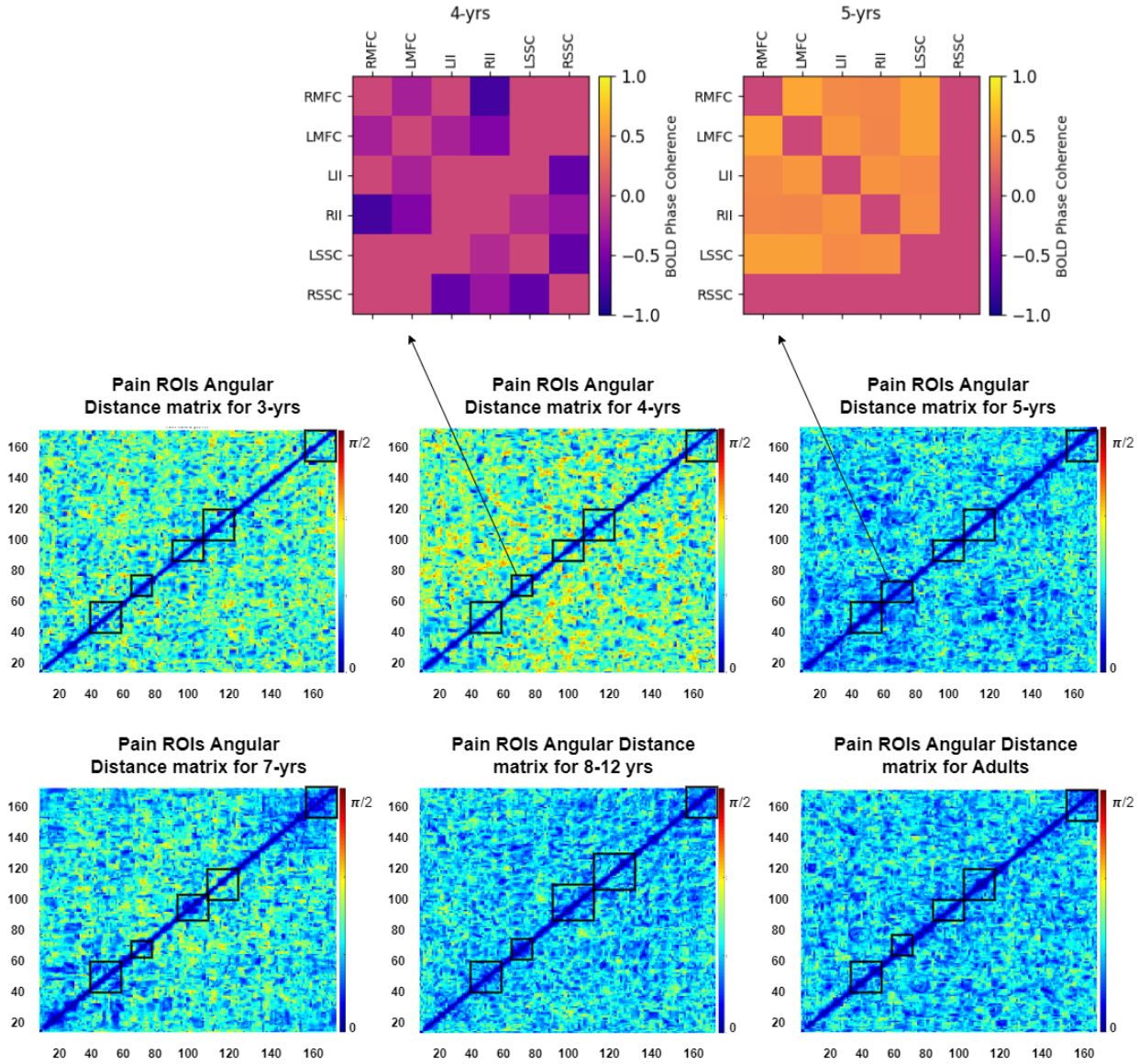

Figure 3.6: Angular distance matrices depicting temporal patterns of pain network ROIs separately for each of the six age groups (3, 4, 5, 7, 8-12 yrs and Adults age groups) (maximum activation in pain network =35-49, 78-85, 88-92, 104-115, 159-168). We observed longer-lived local spread temporal stability patterns for defined time courses in the pain network for 3-yrs to adulthood.

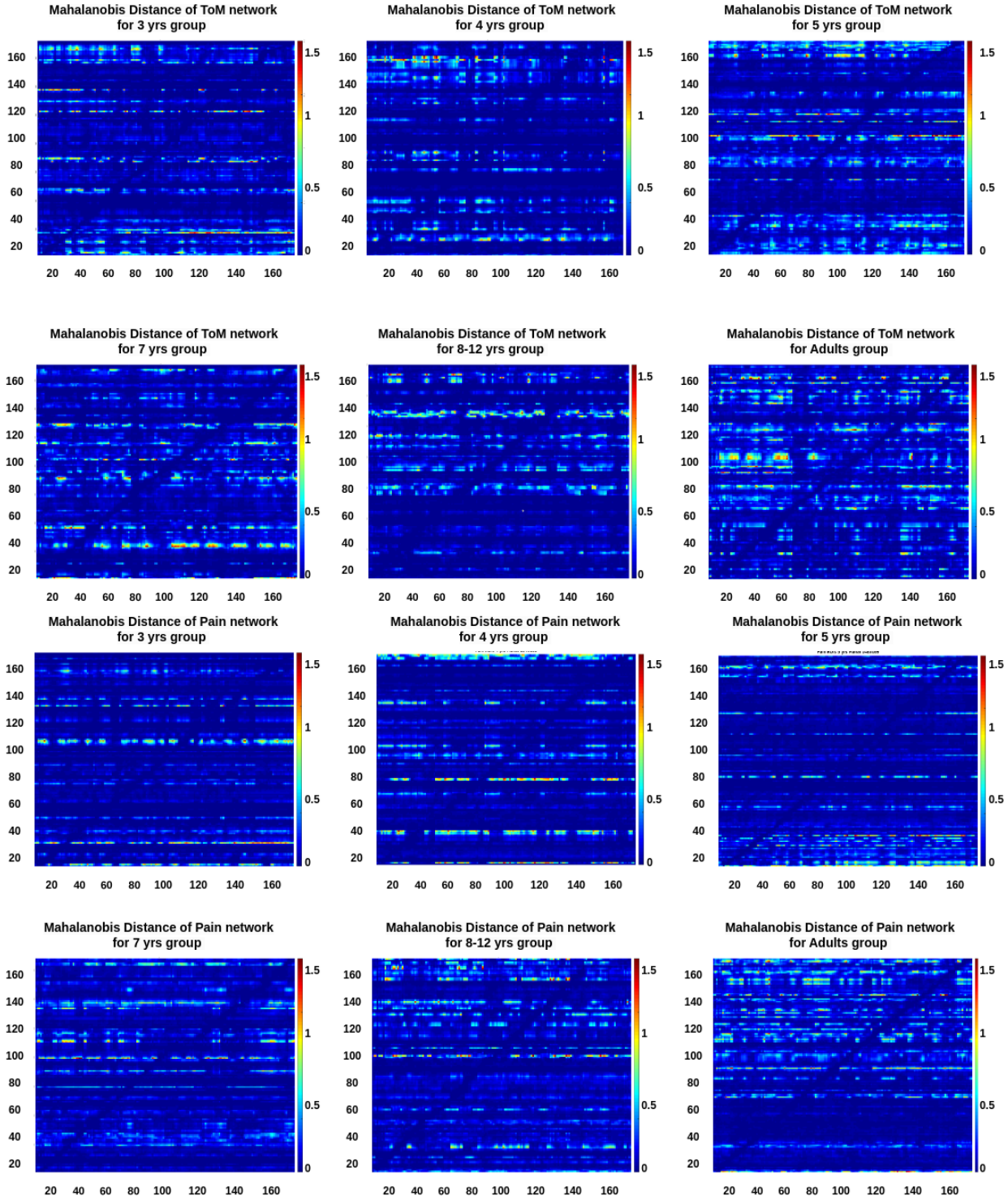

Figure 3.7: Mahalanobis distance matrices depicting temporal patterns of ToM and pain network ROIs for each of the six age groups (3, 4, 5, 7, 8-12 yrs and Adults age groups). We observe a trend of decreasing high distance values to lower overall distance values from children to adults.

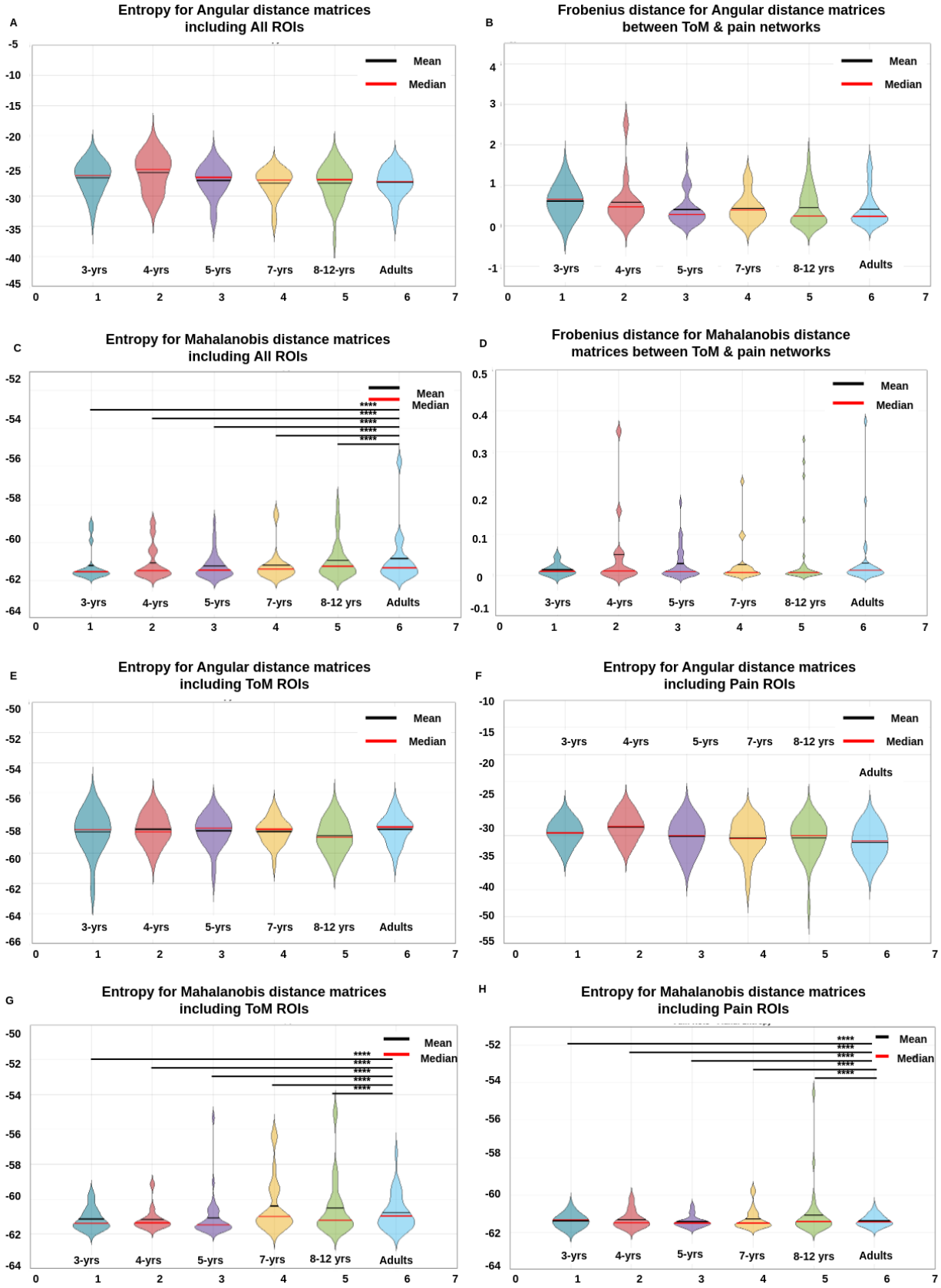

Figure 3.8: Entropy and Frobenius distances matrices: **A and C** are showing entropy for Angular and Mahalanobid distances including All ROIs, whereas **B and D** are depicting Frobenius distance between ToM and Pain ROIs for Angular and Mahalanobis distance. **E,F,G, and H** are showing entopy for Angular and Mahalanobis distance for ToM and Pain ROIs separately. Statistically significant differences are represented using $*(P \leq 0.05)$, $**(P \leq 0.01)$, $***(P \leq 0.001)$, $****(P \leq 0.0001)$, ns (not significant).

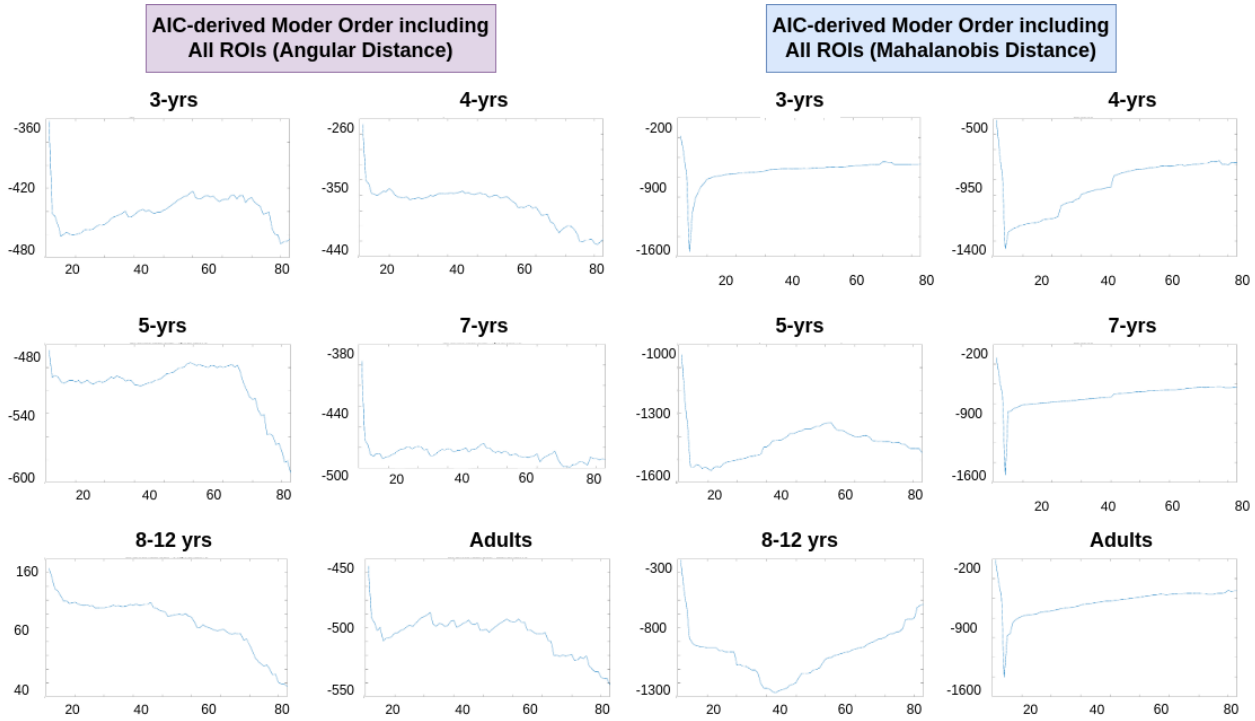

Figure 3.9: Stochastic characteristics of dFC. The figure shows the principal angle, $\phi(t)$, modeled as an autoregressive $AR(\rho)$ process in stochastic modeling. The value of the model order ρ was systematically changed from 0 to 100. The graphic displays the AIC values associated with the model order. The inset shows the initial minimum value of the AIC (Akaike Information Criterion) and the matching model order. . We observe the best fit model for $\rho \geq 2$.

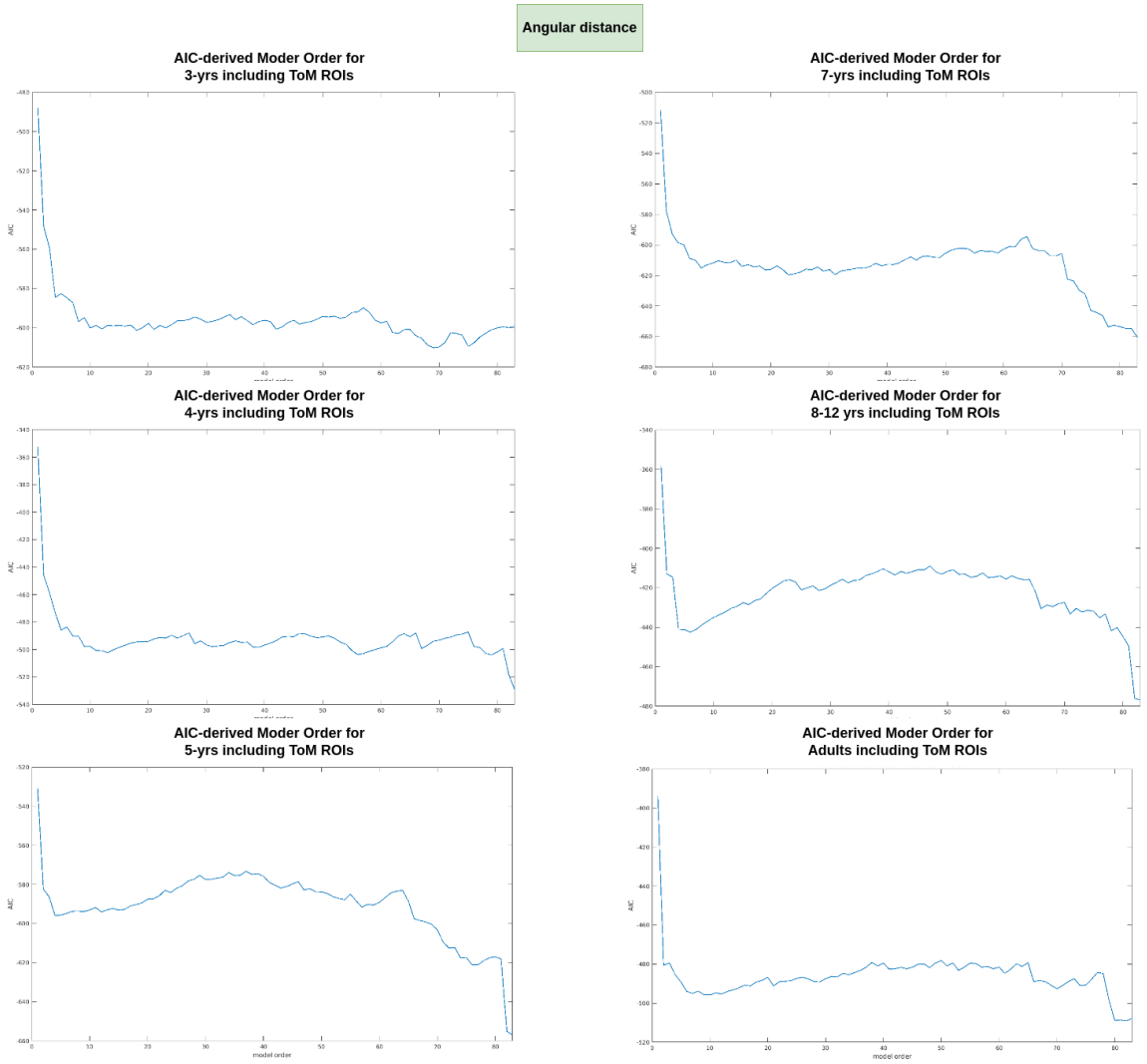

Figure 3.10: AIC matrices for ToM Network in six-groups analysis, for Angular Distance. We observed minimum model order of $\rho \geq 4$ for Angular distance.

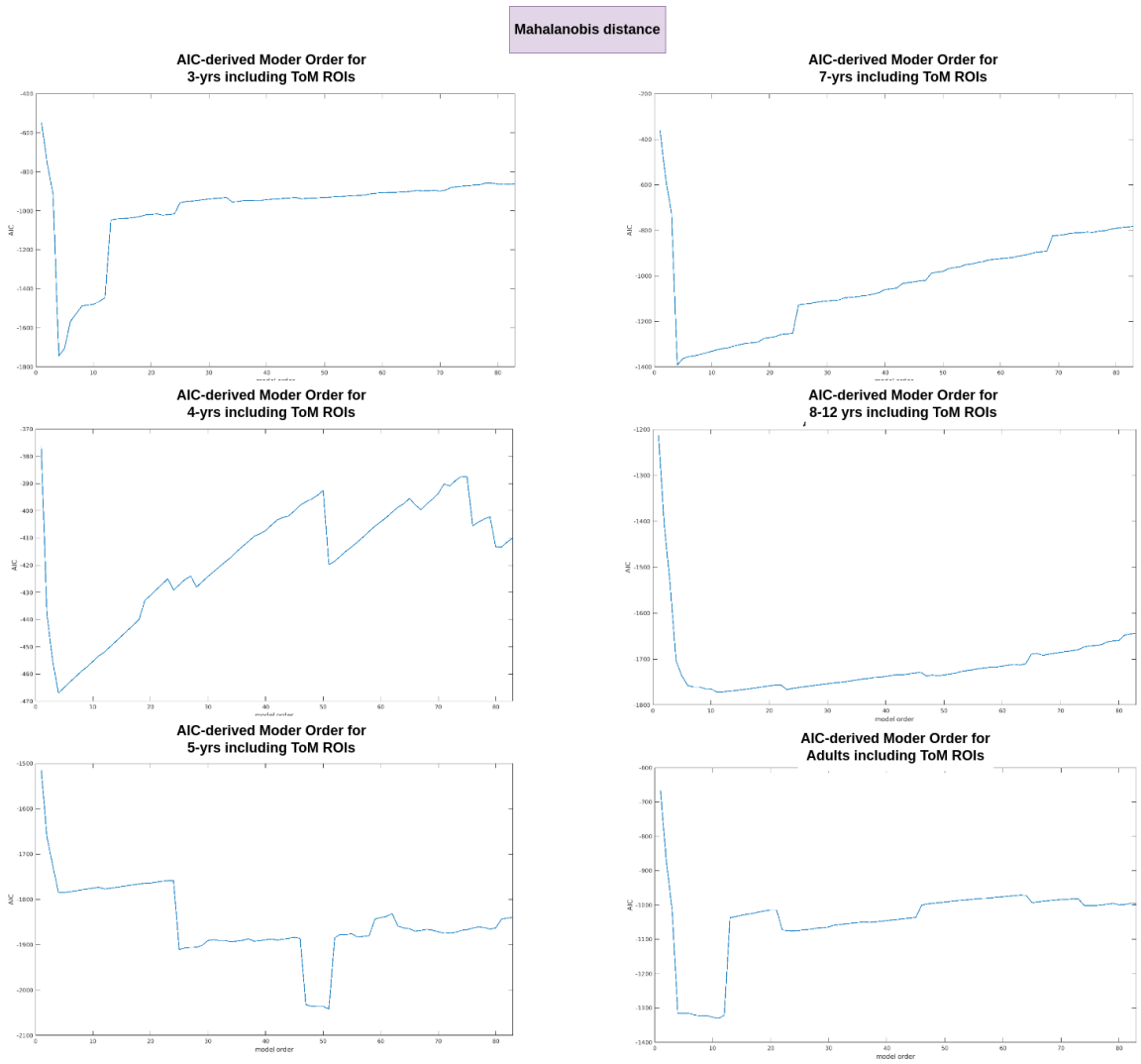

Figure 3.11: AIC matrices for ToM Network in six-groups analysis, for Mahalanobis Distance. We observed minimum model order of $\rho \geq 4$ for Mahalanobis distance.

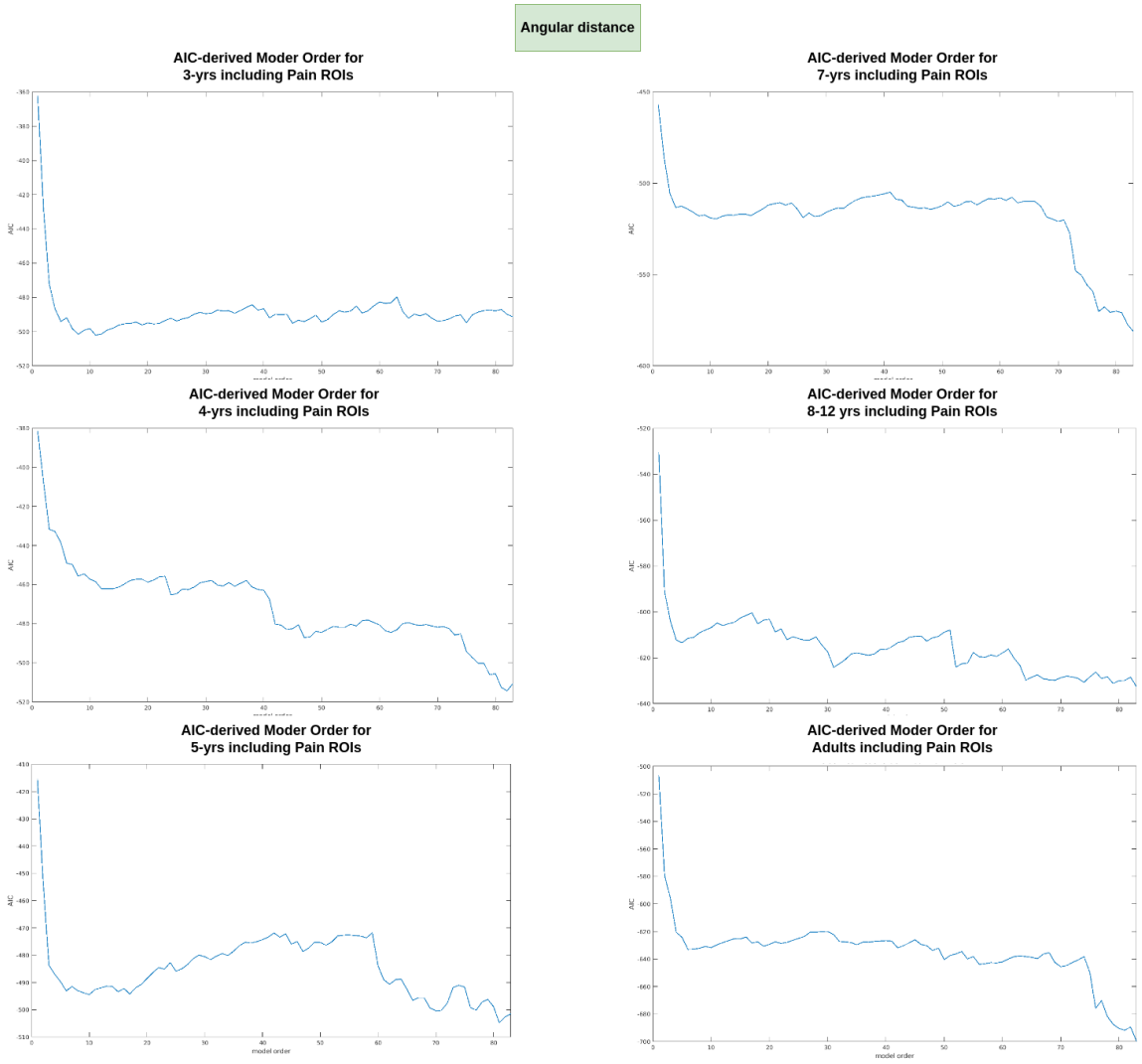

Figure 3.12: AIC matrices for Pain Network in six-groups analysis, for Angular Distance. We observed minimum model order of $\rho \geq 4$ for Angular distance.

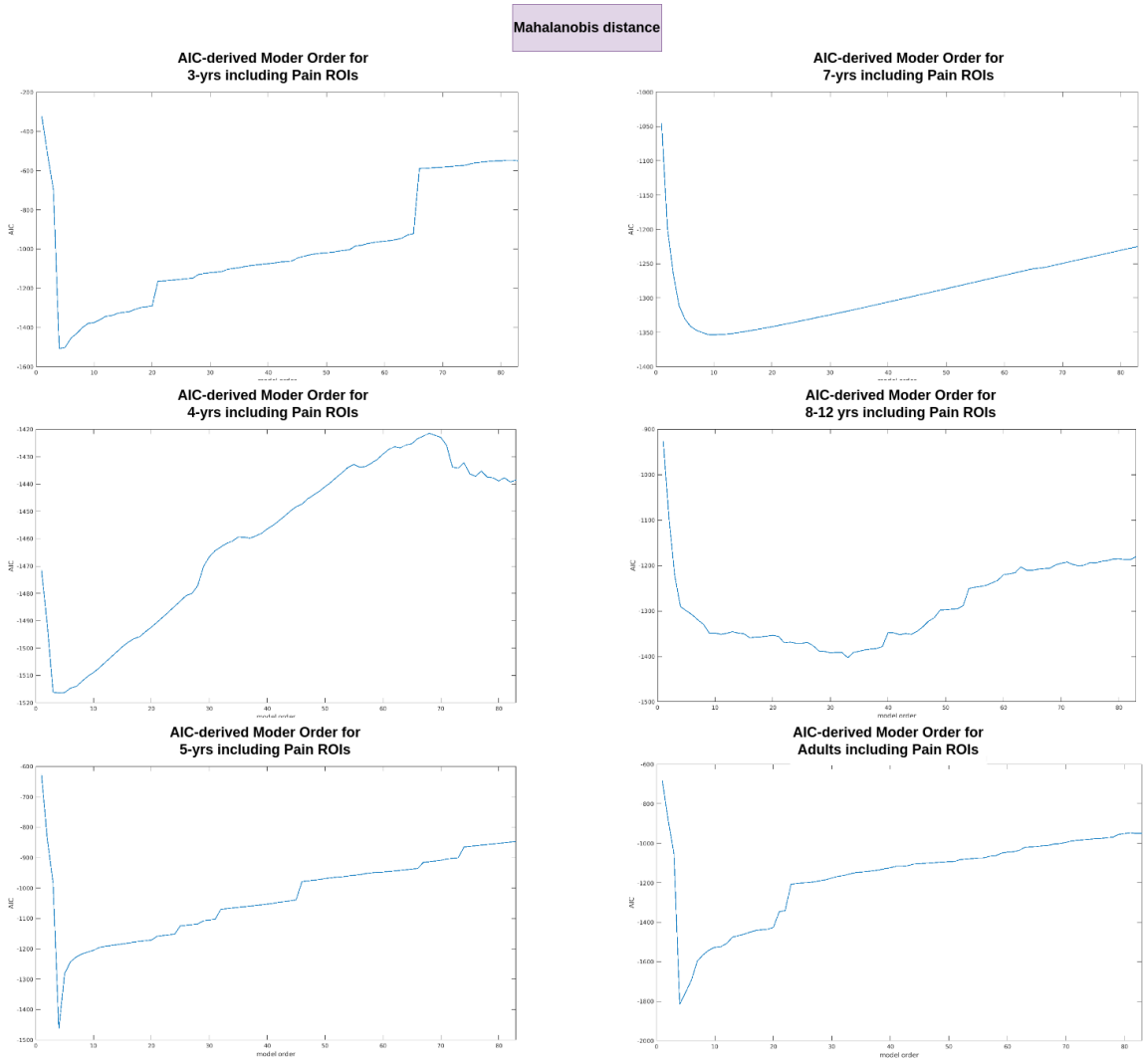

Figure 3.13: AIC matrices for Pain Network in six-groups analysis, for Mahalanobis Distance. We observed minimum model order of $\rho \geq 4$ for Mahalanobis distance.

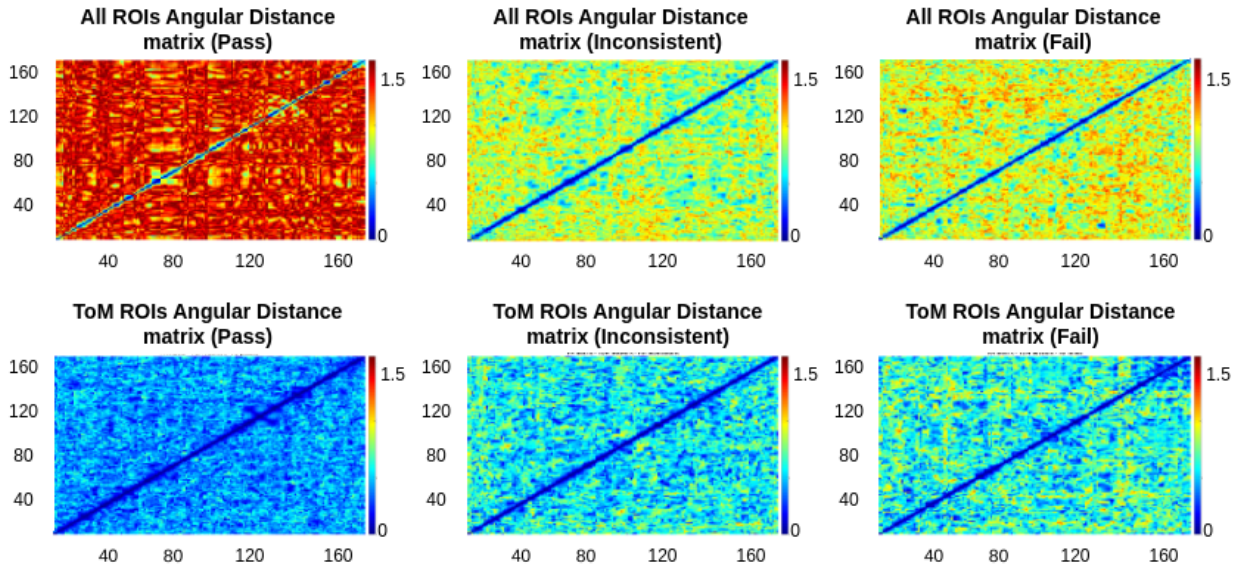

Figure 3.14: Angular distance matrices depicting temporal patterns for false-belief task-based pass, fail, and inconsistent groups. It showed false-belief task is dependent on temporal stability. The figure shows higher temporal stability in ToM network for the pass group, moderate stability for the inconsistent group, and lowest temporal stability for the fail group.

better understand the relationship between temporal stability and ToM development without the confounding effect of age. To validate our hypothesis and get more nuanced insight, we performed temporal stability analysis for false belief task performers. For the participants who passed ToM task, their temporal stability was high for ToM network with low angular distance. In contrast, participants who failed the task' temporal stability was low for ToM network with high angular distance (refer to Figures 7.6 and 7.7).

1. **Temporal Stability using Angular Distance:** A qualitative analysis of the angular distance matrices for the three false-belief task performances (Figure 10) reveals a lower switching in dFC states and higher temporal stability for passers when all and only ToM ROIs are considered. This pattern destabilizes with higher distance values are seen for inconsistent performers, and the fail group has the highest instability (Refer to Figures 7 and 8).

   To quantify differences between temporal matrices, the distance values were converted into Z-scores, and Kolmogorov-Smirnov tests for equality of distributions (all groups were found to have unequal distributions with p varying from < 0.4 to $< 4 \times 10^{-313}$), followed by Kruskal Wallis tests were conducted: All ROIs $\chi^2(2) = 7.31$, $p < 0.03$; Pain ROIs $\chi^2(2) = 15.63$, $p < 0.0005$; ToM ROIs $\chi^2(2) = 12.18$, $p < 0.003$. Dunn-Sidak posthoc test was performed for pairwise comparisons: All ROIs: Pass-Fail: diff=-533.0409, $p = 0.0271$; Pain ROIs: Pass-Inc: diff=-524.7799, $p = 0.0302$, Pass-Fail: diff=-806.1150, $p = 2.8977 \times 10^{-4}$; ToM ROIs: Pass-Fail: diff=-722.1818, $p = 0.0014$; rest NS.

   To quantify the complexity of these temporal stability patterns, entropy was calculated. Kolmogorov-Smirnov test was performed to check for equality of distributions (all groups were found to have unequal distributions with $p < 0.05$), followed by the Kruskal Wallis tests with non-significant results at 5% confidence level (All ROIs $\chi^2(2) = 1.38$, $p < 0.6$; Pain ROIs $\chi^2(2) = 2.11$, $p < 0.4$; ToM ROIs $\chi^2(2) = 2.11$, $p < 0.8$).

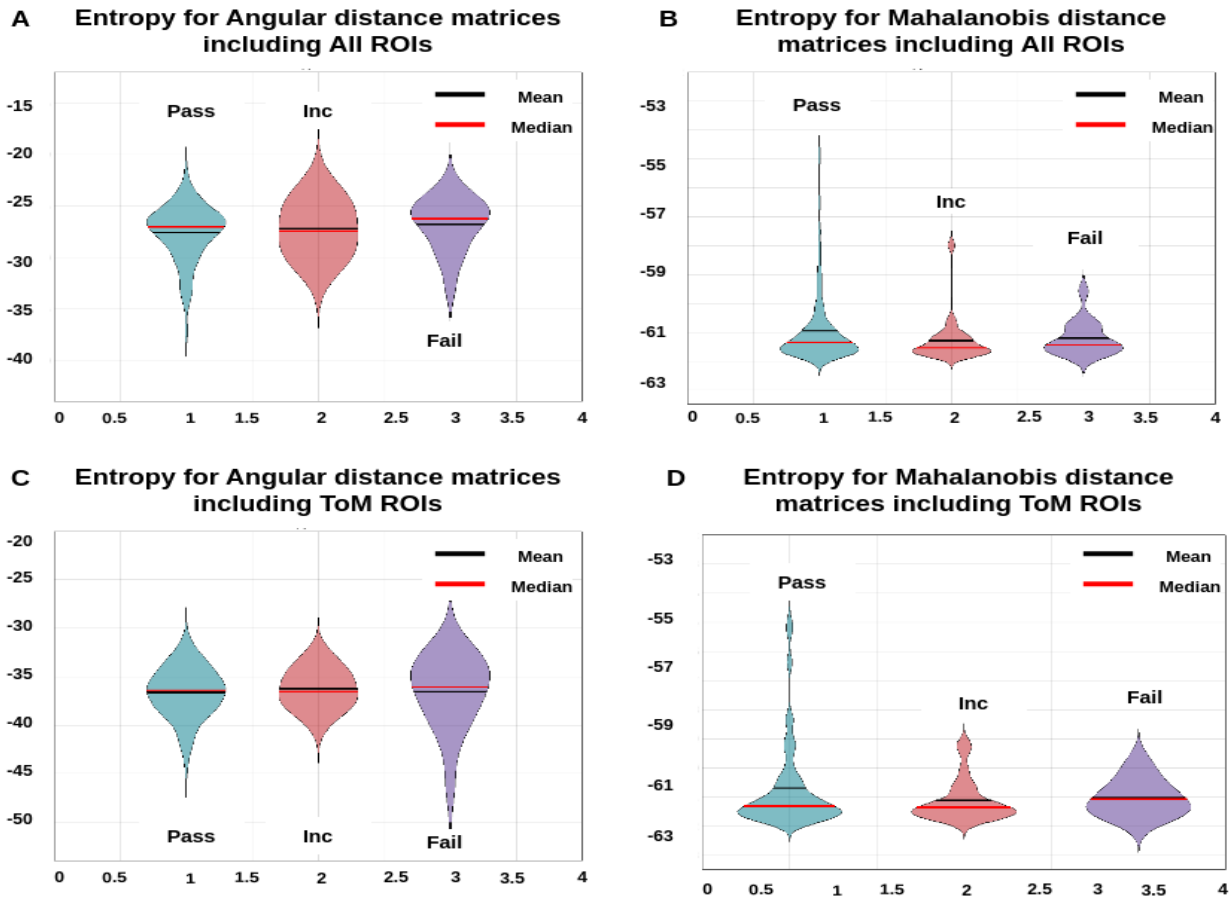

Figure 3.15: **A, C, E** depicts entropy plots for angular distance for the false-belief task-based pass, fail, and inconsistent groups. **B, D, F** are depicting entropy plots for Mahalanobis distance. In the case of entropy plots, Mahalanobis distance is better at capturing the differences in temporal stability in different groups.

2. **Temporal Stability using Mahalanobis Distance:** Qualitative analysis of the Mahalanobis distance matrices reveals no differences for the False-Belief performances.

   We calculated Z-scores for comparing the temporal matrices of pass, fail, and inconsistent groups; the Kolmogorov-Smirnov test was performed, followed by Kruskal-Wallis (All ROIs $\chi^2(2) = 3171.04$, p = 0; Pain ROIs $\chi^2(2) = 5558.54$, p = 0; ToM ROIs $\chi^2(2) = 4777.35$, p = 0) and Dunn-Sidak tests (Refer to Table 3). We also calculated entropy and found that there is an increasing trend for the false-belief test performers, denoting increasing instability from passers to inconsistent performers and failers. To check equality of distribution, we performed the Kolmogorov-Smirnov test and found all false-belief task groups with unequal distribution with $p < 0.05$ (All ROIs $\chi^2(2) = 0.61$, $p < 0.75$; Pain ROIs $\chi^2(2) = 0.57$, $p < 0.8$; ToM ROIs $\chi^2(2) = 0.71$, $p < 0.75$).

3.4 DISCUSSION

In early life, children's brains and cognitive capacities go through significant changes in the first few years of life. For example, in social cognition, young infants acquire a remarkably sophisticated understanding of others' intentions, ideas, and emotions, as opposed to their physiological effects, sensations, pain, hunger, and body states; a vast majority of this development happens before children begin conventional education at the age of six years Richardson *et al.* [2018]; Schult and Wellman [1997]; Schulz *et al.* [2007]; Cohen *et al.* [2011]; **?**. The main objective of this study was to use a naturalistic movie-viewing task that activates the ToM and other functional brain network activations to characterize the temporal stability and fluctuations across developmental age groups specifically for children in the age range of 3-12 yrs. Using a short, engaging, and naturalistic movie stimulus, functional data was acquired from a large sample of children (n=122), including 65 children between 3 and 5 years of age. The movie stimulus used in this study for DFC analysis of fMRI BOLD signals, Pixar's 'Partly Cloudy,' depicts multiple events that focus on two aspects of the main characters (a cloud named Gus and his stork friend Peck): their bodily sensations (often physical pain) and their mental states (beliefs, desires, and emotions) were salient events that drive developmental change and temporal fluctuations in cortical networks recruited for reasoning about bodies (the pain matrix) and minds (the theory of mind network). Additionally, to identify the age range where reasonable temporal stability was achieved and gradually becoming temporally stable over time (especially for adults). Reasonable temporal stability refers to the point at which DFC patterns show consistent and less fluctuating connectivity states over extended periods, indicating mature and stable brain network functioning. Moreover, we hypothesized that there could be a significant association between the temporal stability of DFC patterns of functional brain networks and the behavioral performance in children across different ages, i.e., temporal stability could be associated with the performance of false belief task-based groups. The participants aged 3 to 12 and adults watched a short animated movie (naturalistic stimuli). The previous study reported that Richardson *et al.* [2018], the movie elicited a significant response from ToM and Pain sensory networks at specific time points, as demonstrated by our results. The dataset was first segmented into 3-yrs, 4-yrs, 5-yrs, 7-yrs, 8-12 yrs, and adults to characterize temporal stability differences across ages to address the fluctuation and stochasticity of DFC with development. Subsequently, we used to pass, fail, and inconsistent groups in the behavioral task to check the association between temporal stability and success in explicit false belief task performance.

3.4.1 Stochastic properties of dynamic functional connectivity and age effects in children

The first hypothesis was to characterize the overlap and distinct patterns of temporal stability of dynamic functional connectivity within ToM and pain functional brain networks in 3-12 yrs old children and adults. A previous study has employed within- and between-network static functional connectivity analysis to characterize age-associated developmental differences in segregation and integration in ToM and Pain networks in 3-12 yrs old children Richardson *et al.* [2018]. In the present study, we first apply a data-driven, unsupervised approach to characterize the high-dimensional DFC into lower-dimensional patterns by identifying similar dominant FC configurations over certain temporal segments beyond the previously employed methods. Our method allows a stochastic characterization of functional connectivity for salient events in the movie and fluctuation of dynamic configurations over the relevant time points, suggesting segregation and integration of functional brain networks over time. Subsequently, using 2 different measures—Angular and Mahalanobis distances applied on DFCs extracted across time, we capture the stability of DFC through the temporal stability matrices that could be used to draw critical insights about underlying functional brain states. The central idea is that they are considered stable if the dominant FC configurations are similar for extended time points. For empirical validation, we explored modifications in temporal stability matrices across six different age groups: 3-yrs, 4-yrs, 5-yrs, 7-yrs, 8-12 yrs, and adults as a control group. For six age subgroups, we employed two methods based on the angular distance and Mahalanobis distance: one included all ROIs (Total of 12); the other took individual networks into account (analysis for ToM and Pain network separately). We found a trend of decreasing angular distance and increasing stability from 3-yrs to the adults, with 4-yrs and 7-yrs showing anomalously higher angular distance and instability in the overall trend, and 5-yrs exhibiting a pattern similar to that of 8-12 yrs age group. The increasing stability of higher-cognition and associative brain regions (included in the ToM and Pain networks, respectively) are useful in conferring adaptability and increased capacity to coordinate information processing across the relevant functional networks Li *et al.* [2020a]; Cole *et al.* [2010]; Dehaene *et al.* [2021]. Applying our unsupervised method on movie task-specific brain networks revealed significant differences in temporal stability at different ages during development. Further, It allowed us to identify how ToM network stability patterns at each age shape the age-associated pattern difference. Moreover, our results suggest higher stability, fewer fluctuations, and a capacity to mentalize already developed by the age of 5-yrs in these children. This trend was not statistically significant in the Mahalanobis Distance measure of DFC patterns due to the presence of outliers. The temporal matrices per age group display higher distance values in global patterns for all ROIs than the corresponding matrices for ToM or Pain ROIs, and this difference persists across increasing age. This could demonstrate the distinctive functioning of ToM and Pain networks from as early as 3-yrs of age. Finally, we examined the stochastic properties of temporal stability matrices using auto-regressive modeling. motivated by a few recent findings showing dynamic switching between brain networks and time spent visiting distinct brain networks is not random Marusak *et al.* [2017]; **?**. Subsequently, another recent study has shown that the switching dynamics of functional brain states in the resting state follows the AR model of order 1, or in other words, a Markovian process fully explains the DFC evolution when correlation was computed using a sliding window approach **?**. By constructing the unsupervised temporal stability matrices from 2 alternative approaches—principal angle and Mahalanobis distance, we reveal that DFC evolution is neither random nor Markovian.

3.4.2 Aging introduces temporal variability in the evolution of dynamic functional connectivity ToM and Pain functional brain networks during movie watching

The previous study Richardson *et al.* [2018] reported that the ToM and pain networks are functionally distinct by age 3-yrs, and functional specialization increases throughout childhood. Recent studies also suggest that DFC of neurocognitive networks in children displays age-related increases in temporal variability of FC among neurocognitive networks. These findings lay the groundwork for understanding how variation in the developing functional network dynamics is related to risk for neurodevelopmental disorders Harlalka *et al.* [2019]; Marusak *et al.* [2017]; **?**]; **?**]; Roy and Uddin [2021]. To compare results with the dynamic fluctuations in the functional brain networks during development we quantified temporal matrices for all 12 and 6 ROIs anchored in ToM and Pain functional brain networks. The higher the value of angular distance, the bigger the leap between two dominant DFC subspaces at different time points tx and ty. Temporal stability results for defined time courses (for ToM network (Time-points with maximum activation = 18-27, 82-90, 92-102, 140-149, 150-159) and pain networks (time points with maximum activation =35-49, 78-85, 88-92, 104-115, 159-168) (total of ten time-courses)) for all ROIs, capturing variability between these functional networks, We discovered shorter-lived repeated patterns of temporal stability for 3-yrs and 4-yrs age groups. In contrast, for other age groups, i.e., 5-yrs, 7-yrs, 8-12 yrs, and adults, we found longer-lived temporal stability patterns for defined time courses suggesting an age-associated increase in temporal stability and lesser transient switching of functional connectivity patterns. These results complement prior studies in adults that suggest that ToM brain region selectivity increases with age. To get further insight, we also calculated temporal stability for ToM and pain network separately to check variability within the network. We found longer-lived temporal stability patterns for defined time courses in the ToM network, even for 3-yrs and 4-yrs age groups, and it continued till adulthood. We observed shorter-lived repeated patterns of temporal stability for 3-yrs and 4-yrs age groups in the pain network. We found a change in the stability pattern from the 5-yrs age group (i.e., longer-lived stability pattern) that continued till adulthood. The temporal matrices per age group show higher distance values for All ROIs than the corresponding matrices for ToM or Pain ROIs, and this difference persists through age. Our results for 3-yrs and 4-yrs age groups complement previous findings reporting regions in these two networks were uncorrelated based on FC in the 3-yrs old; however, they were robustly anti-correlated in older children and adults (FC of ToM and Pain matrix). Change in the temporal stability patterns from the 5-yrs group predicted the maturity (i.e., similarity to adults) of each network's distinct temporal fluctuations evoked by the specific movie clips highlighted by time points with maximum activation.

During validation of results using Frobenius Distance analysis, we find the lowest distance between ToM and Pain network activation patterns for 7-yrs, followed by moderately lower values for 5-yrs, 8-12-yrs, and Adults, with high Frobenius Distance value for 3-yrs, and the highest value for 4 y-rs. Frobenius norm was used to measure the differences between the temporal stability matrices computed for ToM and Pain networks. Hence, higher Frobenius norms in 3 and 4-yrs compared with 5-yrs, 7-yrs, 8-12 yrs, and adults argue for developmental differences in ToM and Pain networks. ToM and Pain networks' temporal stability of DFC patterns are more similar between 5-yrs, and adults predicted the maturity (i.e., similarity to adults).

3.4.3 Association between performance on false belief tasks in children and Temporal Stability of DFC in ToM functional brain networks

The second major goal of this study was to ask how the temporal stability of DFC patterns in the ToM network relates to children's theory of mind cognitive abilities. In this context, the behavioural data used in this analysis comprises questions about other people's actions, beliefs,

desires, expectations, and moral blameworthiness. Within this set of questions, six focused on predicting and explaining actions based on false beliefs. Compared to the previous fMRI studies of ToM, the sample included in this paper had a substantial number of children who systematically failed explicit false belief tests. Hence, this allowed us to test for signatures of temporal stability of DFC of specific functional brain networks that were associated with improved performance on false-beliefs tasks. For the false belief performance groups, a lower distance and higher repeatability in patterns were observed for passers, with increasing distances and instability observed for those who failed. Our results are consistent with previous findings that passing false belief tasks was associated with increased functional correlations among regions in the ToM network. This further suggests that increased functional correlations in the ToM network may drive the stability of DFC patterns and may be associated with age. This contrasts with previous findings focusing specifically on 3- to 5-yrs old children, reporting that the neural responses are very similar to social movies in children who systematically fail versus pass explicit false belief tasks. However, our dynamic FC analysis captured subtle variations and nuanced findings that were missed by previous analyses.

Our results are consistent with the existing literature, as at the early childhood stage, ToM and other networks are still developing, and hence, their temporal stability is low. Gradually, these networks become stable with increasing age. The participants who failed the false-beliefs tasks belonged to 3yrs and 4 yrs groups indexed by lower temporal stability. Interestingly, 3-yrs old children who systematically failed false belief tasks recruited ToM brain regions at time points with maximum activation in the movie and as a distinct network from the pain matrix. At the same time, the participants who passed mostly belonged to the 5-yrs age group, where we observed reasonable temporal stability. To get more clarity, we separately performed temporal stability analysis for pass, inconsistent, and fail groups and observed higher temporal stability for the pass group, moderate temporal stability for the inconsistent group, and low temporal stability for the fail group.

3.5 SUMMARY

In this research, we proposed an architecture to examine the developmental changes in temporal stability of ToM and pain networks using a dynamic functional connectivity approach throughout childhood to adolescence. The outcomes of the study suggested that ToM network gets temporal stability at age of 3 yrs, whereas more reasonable temporal stability is at age of 5 yrs, and same pattern for pain sensory network. We were getting more temporal stability for ToM and pain networks for some particular time points where activation was very high. Brain networks are not properly segregated from each other at early childhood stage, it gets more specialized over time. According to our observation, this might be the reason why we were getting low temporal stability at early childhood stage. The current findings are novel, as there is no such method in which temporal stability has been calculated from the early childhood stage, as well as could also be associated with the behavior of the false belief task. There are a few significant limitations of this study, which are as follows: 1) Size of dataset; we used a dataset that contained 155 subjects. In the future, we will include dataset with large no. of samples with different tasks. 2) Tested proposed architecture only in healthy participants. In the future, we will try to include participants suffering from neurological disorders (like autism, ADHD, etc.), so there might be some correlation that remains an open question for the future.